Undergraduate Research Experience Program
Research Reports

Indiana University, Bloomington

Summer 2015

Contents

Preface

During the summer of 2015 five students participated in the Undergraduate Research Experience program in Mathematics at Indiana University. This program was sponsored by Indiana University and the Department of Mathematics. The program ran for eight weeks, from June 7 through July 31, 2015. Five faculty served as research advisers to the students from Indiana University:

- Chris Connell worked with Ben Briggs.
- Kevin Pilgrim worked with Sarah Butchko.
- Dylan Thurston worked with Andrew Henderson.
- Jeffrey Meier worked with Samuel Pilgrim.
- Matt Bainbridge worked with Zachary Wampler.

Following the introductory pizza party, students began meeting with their faculty mentors and continued to do so throughout the next eight weeks. The students also participated in a number of social events and educational opportunities and field trips.

Individual faculty gave talks throughout the program on their research, about two a week. Students also received LaTeX training in a series of workshops. Other opportunities included the option to participate in a GRE and subject test preparation seminar. Additional educational activities included tours of the library, the Slocum puzzle collection at the Lilly Library and the IU cyclotron facility, and self guided tours of the art museum. Students presented their work to faculty mentors and their peers at various times. This culminated in their presentations both in poster form and in talks at the statewide Indiana Summer Undergraduate Research conference which we hosted at the Bloomington campus of IU.

On the lighter side, students were treated to a reception by the graduate school as well as the opportunity to a fun filled trip to a local amusement park. They were also given the opportunity to enjoy a night of "laser tag" courtesy of Prof. Elizabeth Housworth.

The summer REU program required the help and support of many different groups and individuals to make it a success. We foremost thank the Indiana University and the Department of Mathematics for major financial support for this bridge year between two National Science Foundation grants. We especially thank our staff member Mandie McCarty for coordinating the complex logistical arrangments (housing, paychecks, information packets, meal plans, frequent shopping for snacks). Additional logistical support was provided by the Department of Mathematics and our chair, Elizabeth Housworth. We are in particular thankful to Jeff Taylor for the computer support he provided. We thank Indiana graduate student Anne Carter for serving as our LaTeX consultant and for compiling this volume. Thanks to those faculty who served as mentors and those who gave lectures. Thanks to David Baxter of the Center for Exploration

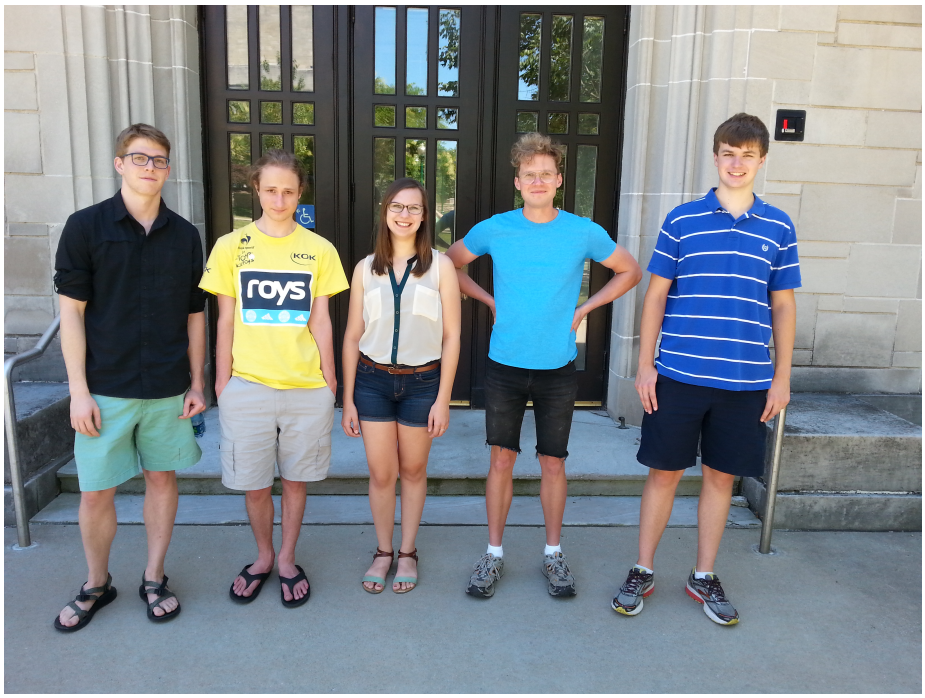

Figure 1: REU Participants, from left to right: Ben Briggs, Sam Pilgrim, Sarah Butchko, Zachary Wampler, Andrew Henderson.

of Energy and Matter (nee IU cyclotron facility) for his personal tour of the cyclotron facility and lecture. Thanks to Andrew Rhoda for his tour of the Slocum puzzle collection.

Chris Connell
September, 2015

Embedding Negetively Curved Surfaces

*Ben Briggs**

Contents

List of Figures

List of Tables

Abstract

We consider the problem of embedding an everywhere negatively curved, regular and intrinsically complete surface, S, in $B_0(1) \in \mathbb{R}^3$. By modifying a construction of Rozendorn's ([Ro66])we reduce the problem to two parts: a topological index manipulation and an embedding problem of patches. The first part having been resolved leaves a constrained PDE system whose solution corresponds to a patch embedding. We then extend this patch embedding solution to a global embedding by an iterative scheme, producing our target surface.
An upshot of this iterative patch embedding method is the existence of everywhere negatively curved surfaces of arbitrary genus with only cusp ends.

1 Background on Curvature

The purpose of this section is to familiarize the reader with technical aspects of differential geometry that play vital roles in embedding problems. This section assumes no familiarity with differential geometry beyond typical methods of multivariable calculus.

1.1 Introducing Surfaces

"Surfaces" admit a large family of definitions, several of which you may be familiar with. For our purposes the following definitions will suffice (see [doC76]).

Definition 1 (Surface)**.** Given $S \subset \mathbb{R}^3$, suppose at every point $p \in S$ there exists a neighborhood $V \subset S$, a open patch $\mathbf{U} \subset \mathbb{R}^2$ and a differentiable map $\boldsymbol{X} : \mathbf{U} \to \mathbb{R}^3$ s.t. $\boldsymbol{X}(\mathbf{U}) = V$. Then S is a surface so long as $\boldsymbol{X}$ has a continuous inverse $\boldsymbol{X}^{-1} : V \subset S \to U \subset \mathbb{R}^2$.

Remark 1. Note that I haven't specified *how* differentiable $\mathbf{X}$ is. Take it to be "smooth", i.e differentiable enough to admit any of the operations we want to perform on it.

Much of what we do requires our surface S to be *regular*. This property is defined as follows.

Definition 2 (Regular Surface)**.** A surface S, locally parameterized by a differentiable map $\mathbf{X} : \mathbf{U} \to \mathbb{R}^3$ is *regular* if $\forall\, p \in S$ d$\mathbf{X}$ is injective. i.e $\frac{\partial \boldsymbol{X}}{\partial u}, \frac{\partial \boldsymbol{X}}{\partial v}$ are linearly independant.

This substantial property will later allow us to repeatedly use the partial derivatives $\frac{\partial \boldsymbol{X}}{\partial u}, \frac{\partial \boldsymbol{X}}{\partial v}$ at a point $p \in S$ as a basis for the tangent space at p, $T_p(S)$.

1.2 Introducing Curvature

In this section, I will introduce some straightfoward notions of curvature and the paradigms which accompany them.

Curve-Curvature in $\mathbb{R}^3$ To begin thinking about curvature, consider a map

$$\boldsymbol{\alpha} : [a, b] \to \mathbb{R}^3 \qquad a, b \in \mathbb{R}$$

Call this map a curve in $\mathbb{R}^3$, and let it be parameterized by it's arc length "s".

Remark 2. It is true that any curve $\alpha : [a, b] \to \mathbb{R}^3$ arbitrarily parameterized can be equivalently parameterized by arc length. The proof of this fact is left to the reader.

We like parameterizing by arc length because it normalizes the derivative function. i.e if $\alpha(s) = \begin{bmatrix} \alpha_x(s) \\ \alpha_y(s) \\ \alpha_z(s) \end{bmatrix}$, then we have

$$\begin{aligned} \left\| \frac{d}{ds}[\alpha(s)] \right\| = \left\| \frac{d}{ds} \begin{bmatrix} \alpha_x(s) \\ \alpha_y(s) \\ \alpha_z(s) \end{bmatrix} \right\| &= \left\| \begin{bmatrix} \frac{d\alpha_x(s)}{ds} \\ \frac{d\alpha_y(s)}{ds} \\ \frac{d\alpha_z(s)}{ds} \end{bmatrix} \right\| \\ &= \sqrt{\frac{d\alpha_x(s)^2 + d\alpha_y(s)^2 + d\alpha_z(s)^2}{ds^2}} = \sqrt{\frac{ds^2}{ds^2}} \\ &= 1 \end{aligned} \tag{1}$$

This insures the second derivative of $\alpha(s)$ only measures the change in direction of the curve, allowing the following definition.

Definition 3 (Curvature)**.** Let a curve $\alpha(s) : [a, b] \to \mathbb{R}^3$ be a differentiable map from an interval [a,b] to $\mathbb{R}^3$, parameterized by arc length s. The number $|\alpha''(s)| = k(s)$ is called the curvature of α at s.

This notion of curvature makes sense; it measures the size of local changes in direction of the tangent space. As we would want, curvature is independent of orientation, and thus is directly a function of position.

Gaussian Curvature Now we will generalize our notion of curvature to surfaces in $\mathbb{R}^3$. We will see similar intuition applies to our definition of Gaussian curvature as applied to curve curvature.

Consider a regular surface S, parameterized by a differentiable function $\boldsymbol{X} : U \to \mathbb{R}^3$, with $U \in \mathbb{R}^2$ a patch with basis $\{u, v\}$. There exists a vector field on S associating each point $p \in S$ with the unit normal vector on S at p. The map defining this vector field is called the Gauss map.

Definition 4 (Gauss Map)**.** Let $S \in \mathbb{R}^3$ be a surface with orientation $\boldsymbol{N}$. The map $\boldsymbol{N} : S \to \mathbb{R}^3$ takes values in the unit sphere

$$S^2 = \{(x, y, z) \in \mathbb{R}^3 \,;\, x^2 + y^2 + z^2 = 1\}$$

and is called the Gauss map.

The regularity of S allows us to formulate the Gauss map in terms of the parameterization, $\boldsymbol{X}$. Writing the partial derivatives of $\boldsymbol{X}$, $\frac{\partial \boldsymbol{X}_p}{\partial u}, \frac{\partial \boldsymbol{X}_p}{\partial v}$ as $\boldsymbol{x}_u, \boldsymbol{x}_v$ respectively, we know $\{\boldsymbol{x}_u, \boldsymbol{x}_v\}$ is a basis of the tangent space at the point p$\in S$, called $T_p(S)$. Then we have

$$\boldsymbol{N}_p := \frac{\boldsymbol{x}_u \wedge \boldsymbol{x}_v}{\|\boldsymbol{x}_u \wedge \boldsymbol{x}_v\|}$$

Where $\wedge$ denotes the cross product.

Looking back to curves, the Gauss map is like the first derivative of $\alpha(s)$; it has normal length, but changes in direction exactly as the tangent space does. Knowing this, you should not be surprised we are interested in the derivative of the Gauss map. To elaborate, notice the differential $d\boldsymbol{N}_p$ takes vectors in $T_p(S)$ to $T_{\boldsymbol{N}(p)}(S^2)$, and since these are parallel planes, we can think of $d\boldsymbol{N}_p$ as a linear transformation

$$d\boldsymbol{N}_p : T_p(S) \to T_p(S)$$

Equivalently, but more explicitly notice

$$\exists\, a, b, c, d \in \mathbb{R} \quad s.t.$$

$$\boldsymbol{N}_u = a\boldsymbol{x}_u + b\boldsymbol{x}_v$$

$$\boldsymbol{N}_v = c\boldsymbol{x}_u + d\boldsymbol{x}_v$$

Thus we can write

$$d\boldsymbol{N}_p = \begin{bmatrix} \boldsymbol{N}_u & \boldsymbol{N}_v \end{bmatrix} = \begin{bmatrix} a & b \\ c & d \end{bmatrix} \begin{bmatrix} \boldsymbol{x}_u \\ \boldsymbol{x}_v \end{bmatrix}$$

Where you can see the matrix $\begin{bmatrix} a & b \\ c & d \end{bmatrix}$ represents a linear transformation $T_p(S) \to T_p(S)$. Finally, we define Gaussian Curvature.

Definition 5 (Gaussian Curvature)**.** Let $p \in S$ and $d\boldsymbol{N}_p : T_p(S) \to T_p(S)$ be the differential of the Gauss map at p. Then the Gaussian Curvature of the surface S at the point p is given by

$$K = det[d\boldsymbol{N}_p]$$

To see why we choose this definition, consider the following. For a unit vector $\overrightarrow{w} \in T_p(S)$, $d\boldsymbol{N}_p(\overrightarrow{w})$ is the local change of N in the direction $\overrightarrow{w}$. So we should understand the action of the linear transformation $d\boldsymbol{N}_p : T_p(S) \to T_p(S)$ on the basis $\{\boldsymbol{x}_u, \boldsymbol{x}_v\}$ to completely describe the local change in the normal vector (and consequently the tangent plane). The determinant of a linear transformation is the scale factor associated with the transformation's volumetric effect on a paralellogram, and we can think of the basis $\{\boldsymbol{x}_u, \boldsymbol{x}_v\}$ as a parallelogram. Thus we see the determinant of $d\boldsymbol{N}_p$ measures the scale of local changes in the tangent space.

Principle Curvature We know the linear transformation $d\boldsymbol{N}_p$ has two or more associated eigendirections. If v is an eigenvector of the matrix $d\boldsymbol{N}_p$ then

$$d\boldsymbol{N}_p v = \lambda v \quad \lambda \in \mathbb{R}$$

Which we can take to mean, at a point p $\in S$, there are at least two directions along which the position change and the normal direction change are parallel.

These are called the *principle curvature directions*. Curves which travel everywhere tangent to principle directions are called principle curves. Of all curves on S through p, the principle curves have the maximum and minimum normal curvatures. Moreover, these curvatures are the eigenvalues associated with the given eigendirections. Thus we have

Theorem 1. *Let S be a surface with a point p, and Gauss map $\boldsymbol{N}_p$ at p. Let the normal curvatures of the principles curves be k_1 and k_2. Then k_1 and k_2 are eigenvalues of $d\boldsymbol{N}_p$ and*

$$K = det[d\boldsymbol{N}_p] = k_1 k_2$$

1.3 Fundamental Forms

This section introduces two vital geometric objects known as the first and second fundamental forms. Their meanings are closely related to the distinction between intrinsic and extrinsic geometry. So before formally defining the first and second fundamental forms we will characterize this distinction.

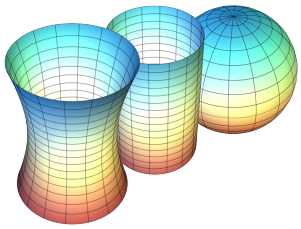

Figure 1: A hyperboloid, a cylinder and a sphere with $K < 0$, $K = 0$ and $K > 0$ respectively.

Intrinsic Geometry The distinction between instrinsic and extrinsic viewpoints is often explained in the following way: imagine you are a two dimensional person living inside of a surface. Properties of the surface which are distinguishable to you should viewed as instrinsic. In particular, your ability to distinguish various surfaces (were you able to travel) should define intrinsic equivalence classes on the set of surfaces. As an aide you can imagine that any surface which can be laid on top of another without stretching is intrinsically identical to the other, such as a half pipe and a plane. Briefly, it is accurate to say that any properties of a surface which are determined solely by distances or angles within the surface are intrinsic properties.

Extrinsic Geometry The extrinsic viewpoint is more discerning, distinguishing intrinsically identical surfaces which are differently embedded, for example the half pipe and the plane. Extrinsically two surfaces are only identical if an isometry of $\mathbb{R}^3$ takes one onto the other.

The First Fundamental Form The first fundamental form is associated with intrinsic geometry. It is an object which defines distances on the surface. Given a surface S of arbitrary curvature we can always calculate the length of some curve by integrating over infintesimal line segments along the curve. On increasingly smaller neighborhoods of $p \in S$, S becomes increasingly flat. This leads to $ds = P_{T_p(S)}ds$ where ds is the length of a line segment in an infinitesimally small neighborhood of p and $P_{T_p(S)}ds$ is the projection of ds onto the tangent space at p. So we have for two points, p,q in S, infinitesimally separated by $ds = du + dv$ the distance $d(p, q)$ is equivalent to

$$\sqrt{ds^2} = \sqrt{E\,du^2 + 2F\,du\,dv + G\,dv^2}$$

Collecting coefficients we define the first fundamental form.

Definition 6 (First Fundamental Form)**.** If $ds \subset S$ is an infinitesimal line segment in an arbitrarily small neighborhood of a point $p \in S$. Then the quadratic form corresponding to the squared length of $P_{T_p(S)}ds$ is the First Fundamental Form. I.E:

$$I = E\,du^2 + 2F\,du\,dv + G\,dv^2$$

Conventionally, we treat as this form the associated 2x2 matrix

$$\begin{bmatrix} E & F \\ F & G \end{bmatrix}$$

Moreover, This form is often called the "metric" of a surface.

Significantly, the I-form of S at p can be expressed in terms of the parameterization of S at p.

Theorem 2. *Let $S \subset \mathbb{R}^3$ be a surface parameterized by the map $\boldsymbol{X} : U \in \mathbb{R}^2 \to \mathbb{R}^3$ with the I-form*

$$\begin{bmatrix} E & F \\ F & G \end{bmatrix}$$

at an arbitrary point $p \in S$. We can express the I-form in terms of the parameterization $\boldsymbol{X}$.

$$\begin{bmatrix} E & F \\ F & G \end{bmatrix} = \begin{bmatrix} \langle \boldsymbol{x}_u, \boldsymbol{x}_u \rangle & \langle \boldsymbol{x}_u, \boldsymbol{x}_v \rangle \\ \langle \boldsymbol{x}_v, \boldsymbol{x}_u \rangle & \langle \boldsymbol{x}_v, \boldsymbol{x}_v \rangle \end{bmatrix}$$

where $\langle ., . \rangle$ denotes the Euclidean inner product.

Proof. Let $S \in \mathbb{R}^3$ be a surface parameterized by the map $\boldsymbol{X} : U \in \mathbb{R}^2 \to \mathbb{R}^3$ with a point $p \in S$. The natural inner product of $\mathbb{R}^3$ "induces" an intrinsic inner product on the tangent space $T_p(S)$ by composing with the map that reexpresses points in intrinsic coordinate as identical points in extrinsic coordinates, namely the parameterization. i.e. Vectors $\overrightarrow{q}, \overrightarrow{r} \in T_p(S)$ can be written

$$\begin{aligned} \overrightarrow{q} &= a\boldsymbol{x}_u + b\boldsymbol{x}_v \\ \overrightarrow{r} &= c\boldsymbol{x}_u + d\boldsymbol{x}_v \end{aligned} \tag{2}$$

Writing the Euclidean inner product of these vectors produces

$$\begin{aligned} \langle \overrightarrow{q}, \overrightarrow{r} \rangle &= \langle \begin{bmatrix} \boldsymbol{x}_u & \boldsymbol{x}_v \end{bmatrix} \begin{bmatrix} a \\ b \end{bmatrix}, \begin{bmatrix} \boldsymbol{x}_u & \boldsymbol{x}_v \end{bmatrix} \begin{bmatrix} c \\ d \end{bmatrix} \rangle \\ &= \begin{bmatrix} \boldsymbol{x}_u & \boldsymbol{x}_v \end{bmatrix} \begin{bmatrix} a \\ b \end{bmatrix}^t \begin{bmatrix} \boldsymbol{x}_u & \boldsymbol{x}_v \end{bmatrix} \begin{bmatrix} c \\ d \end{bmatrix} \\ &= \begin{bmatrix} a & b \end{bmatrix} \begin{bmatrix} \boldsymbol{x}_u \\ \boldsymbol{x}_v \end{bmatrix} \begin{bmatrix} \boldsymbol{x}_u & \boldsymbol{x}_v \end{bmatrix} \begin{bmatrix} c \\ d \end{bmatrix} \\ &= \begin{bmatrix} a & b \end{bmatrix} \begin{bmatrix} \langle \boldsymbol{x}_u, \boldsymbol{x}_u \rangle & \langle \boldsymbol{x}_u, \boldsymbol{x}_v \rangle \\ \langle \boldsymbol{x}_v, \boldsymbol{x}_u \rangle & \langle \boldsymbol{x}_v, \boldsymbol{x}_v \rangle \end{bmatrix} \begin{bmatrix} c \\ d \end{bmatrix} \end{aligned} \tag{3}$$

Thus, for an infinitesimal line segment projected onto the tangent plane at p, we have

$$\begin{aligned} \langle ds, ds \rangle &= \begin{bmatrix} dx & dy \end{bmatrix} \begin{bmatrix} \langle \boldsymbol{x}_u, \boldsymbol{x}_u \rangle & \langle \boldsymbol{x}_u, \boldsymbol{x}_v \rangle \\ \langle \boldsymbol{x}_v, \boldsymbol{x}_u \rangle & \langle \boldsymbol{x}_v, \boldsymbol{x}_v \rangle \end{bmatrix} \begin{bmatrix} dx \\ dy \end{bmatrix} \\ &= \langle \boldsymbol{x}_u, \boldsymbol{x}_u \rangle \, dx^2 + 2\langle \boldsymbol{x}_u, \boldsymbol{x}_v \rangle \, dx \, dy + \langle \boldsymbol{x}_v, \boldsymbol{x}_v \rangle \, dy^2 \end{aligned} \tag{4}$$

□

The Second Fundamental Form Predictably, the second fundamental form encodes extrinsic information about the surface S. It does so by tracking the distance between arbitrary infinitesimal vectors in S, based at $p \in S$ and the tangent plane $T_p(S)$.

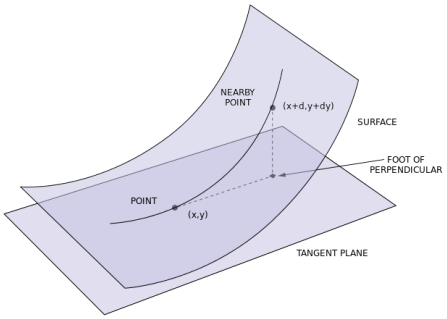

Figure 2: Defining the II-form

Definition 7 (Second Fundamental Form)**.** Let $S \in \mathbb{R}^3$ be a surface and $p = (u, v) \in S, \quad u, v \in \mathbb{R}$ be a point expressed using intrinsic coordinates. Then the distance between a point $p' = (u + du, v + dv)$ and the nearest point on the plane $T_p(S)$ (2) takes the form

$$d(p', T_p(S))) = II = e\,du^2 + 2f\,du\,dv + g\,dv^2$$

and is called the Second Fundamental Form of S at p. As before, there is a conventional matrix form

$$\begin{bmatrix} e & f \\ f & g \end{bmatrix}$$

The form $e\,du^2 + 2f\,du\,dv + g\,dv^2$ is obtained by considering the general polynomial expansion of the surface near p, and restricting the neighborhood until the higher order terms are omittably small.

As it was with the I-form, we have equivalent ways of expressing the II-form.

Theorem 3. *Let $S \subset \mathbb{R}^3$ be a surface with Gauss map $d\boldsymbol{N}_p$ at $p \in S$. The II-form of S at p can be written*

$$\begin{aligned} II_p &= -\langle d\boldsymbol{N}_p(\overrightarrow{w}), \overrightarrow{w}\rangle \qquad \overrightarrow{w} \in T_p(S) \\ &= \begin{bmatrix} \langle \boldsymbol{N}_u, \boldsymbol{x}_u\rangle & \langle \boldsymbol{N}_u, \boldsymbol{x}_v\rangle \\ \langle \boldsymbol{N}_v, \boldsymbol{x}_u\rangle & \langle \boldsymbol{N}_v, \boldsymbol{x}_v\rangle \end{bmatrix} \end{aligned} \tag{5}$$

Proof. Pick an infinitesimal vector $\overrightarrow{w} \in T_p(S)$, then $\exists$ a parameterized curve

$\alpha(s) : [a, b] \to \mathbb{R}^3$ s.t. $\alpha(0) = p$ and $\alpha'(0) = \overrightarrow{w}$. Then we have

$$\begin{aligned} II_p &= -\langle d\boldsymbol{N}_p(\alpha'(0)), \alpha'(0)\rangle \\ &= -\langle \boldsymbol{N}_u\, du + \boldsymbol{N}_v\, dv, \boldsymbol{x}_u\, du + \boldsymbol{x}_v\, dv\rangle \\ &= e\, du^2 + 2f\, du\, dv + g\, dv^2 \end{aligned} \tag{6}$$

Using

$$\begin{aligned} \langle \boldsymbol{N}, \boldsymbol{x}_u\rangle,\, \langle \boldsymbol{N}, \boldsymbol{x}_v\rangle &= 0 \\ \Rightarrow & \\ \langle \boldsymbol{N}_u, \boldsymbol{x}_u\rangle + \langle \boldsymbol{N}, \boldsymbol{x}_{uu}\rangle &= 0 \\ \langle \boldsymbol{N}_v, \boldsymbol{x}_v\rangle + \langle \boldsymbol{N}, \boldsymbol{x}_{vv}\rangle &= 0 \end{aligned} \tag{7}$$

we get

$$\begin{aligned} e &= -\langle \boldsymbol{N}_u, \boldsymbol{x}_u\rangle = \langle \boldsymbol{N}, \boldsymbol{x}_{uu}\rangle \\ f &= -\langle \boldsymbol{N}_u, \boldsymbol{x}_v\rangle = \langle \boldsymbol{N}, \boldsymbol{x}_{uv}\rangle = \langle \boldsymbol{N}, \boldsymbol{x}_{vu}\rangle = -\langle \boldsymbol{N}_v, \boldsymbol{x}_u\rangle \\ g &= -\langle \boldsymbol{N}_v, \boldsymbol{x}_v\rangle = \langle \boldsymbol{N}, \boldsymbol{x}_{vv}\rangle \end{aligned} \tag{8}$$

□

Then there is a somewhat straightforward computation, left to the reader, that produces this significant result.

Theorem 4 (Weingarten Equation)**.** *Let*

$$I_p = \begin{bmatrix} E & F \\ F & G \end{bmatrix} \quad II_p = \begin{bmatrix} e & f \\ f & g \end{bmatrix}$$

be the first and second fundamental forms, respectively, of a surface S at a point p. Then the Gaussian curvature of S at p is given by

$$K = \frac{eg - f^2}{EG - F^2} = \frac{det[II_p]}{det[I_p]}$$

1.4 Gauss, Bonnet and Compatibility

In the following section, we will fill out our understanding of the previously discussed objects with the introduction of several fundamental results. These include the Remarkable Theorem, The Compatibility or "Gauss-Codazzi-Mainardi" equations, and the Bonnet Theorem, otherwise known as the Fundamental Theorem of Surfaces.

Christoffel Symbols This may seem mysterious at first, but bear with me. As always, let S denote a regular surface with parameterization $\boldsymbol{X} : U \subset \mathbb{R}^2 \to S$. Then for all points on S the vectors $\boldsymbol{x}_u, \boldsymbol{x}_v, N$ form a basis. Now take the u and v derivatives of $\boldsymbol{x}_u, \boldsymbol{x}_v$ and express each as linear combinations of the basis vectors with undetermined coefficients, Γ^i_{jk}.

$$\begin{aligned}
\boldsymbol{x}_{uu} &= \Gamma^1_{11}\boldsymbol{x}_u + \Gamma^2_{11}\boldsymbol{x}_v + R_1\boldsymbol{N} \\
\boldsymbol{x}_{uv} &= \Gamma^1_{12}\boldsymbol{x}_u + \Gamma^2_{12}\boldsymbol{x}_v + R_2\boldsymbol{N} \\
\boldsymbol{x}_{vu} &= \Gamma^1_{21}\boldsymbol{x}_u + \Gamma^2_{21}\boldsymbol{x}_v + R_3\boldsymbol{N} \\
\boldsymbol{x}_{vv} &= \Gamma^1_{22}\boldsymbol{x}_u + \Gamma^2_{22}\boldsymbol{x}_v + R_4\boldsymbol{N}
\end{aligned} \tag{9}$$

Now take the inner products of each of these four relations with each of the three basis vectors $\{N, \boldsymbol{x}_u, \boldsymbol{x}_v\}$.

$$\begin{aligned}
&\langle \boldsymbol{N}, \boldsymbol{x}_{uu} \rangle = e = R_1 \\
&\langle \boldsymbol{N}, \boldsymbol{x}_{uv} \rangle = \langle N, \boldsymbol{x}_{vu} \rangle = f = R_2 = R_3 \\
&\langle \boldsymbol{N}, \boldsymbol{x}_{vv} \rangle = g = R_4
\end{aligned} \tag{10}$$

$$\begin{aligned}
\langle \boldsymbol{x}_{uu}, \boldsymbol{x}_u \rangle &= \Gamma^1_{11}E + \Gamma^2_{11}F = \frac{1}{2}E_u \\
\langle \boldsymbol{x}_{uu}, \boldsymbol{x}_v \rangle &= \Gamma^1_{11}F + \Gamma^2_{11}G = F_u - \frac{1}{2}E_v \\
\langle \boldsymbol{x}_{uv}, \boldsymbol{x}_u \rangle &= \Gamma^1_{12}E + \Gamma^2_{12}F = \frac{1}{2}E_v \\
\langle \boldsymbol{x}_{uv}, \boldsymbol{x}_v \rangle &= \Gamma^1_{12}F + \Gamma^2_{12}G = \frac{1}{2}G_u \\
\langle \boldsymbol{x}_{vv}, \boldsymbol{x}_u \rangle &= \Gamma^1_{22}E + \Gamma^2_{22}F = F_v - \frac{1}{2}G_u \\
\langle \boldsymbol{x}_{vv}, \boldsymbol{x}_v \rangle &= \Gamma^1_{22}F + \Gamma^2_{22}G = \frac{1}{2}G_v
\end{aligned} \tag{11}$$

Notice this is a solvable system of equations, thus we can always express these coefficients, hereafter referred to as Christoffel symbols, in terms of the coefficients of the first fundamental form. This fact is significant, and you will see why.

The Remarkable Theorem Continuing with our analysis, we consider the equations

$$\begin{aligned}
(\boldsymbol{x}_{uu})_v - (\boldsymbol{x}_{uv})_u &= 0 \\
(\boldsymbol{x}_{vv})_u + (\boldsymbol{x}vu)_v &= 0 \\
\boldsymbol{N}_{uv} - \boldsymbol{N}_{vu} &= 0
\end{aligned} \tag{12}$$

Using the second derivative expressions in [9], we can rewrite the above formulas as combinations of $\boldsymbol{x}_u, \boldsymbol{x}_v, \boldsymbol{N}$.

$$\begin{aligned} \alpha_1 \boldsymbol{x}_u + \beta_1 \boldsymbol{x}_v + \gamma_1 \boldsymbol{N} &= 0 \\ \alpha_2 \boldsymbol{x}_u + \beta_2 \boldsymbol{x}_v + \gamma_2 \boldsymbol{N} &= 0 \\ \alpha_3 \boldsymbol{x}_u + \beta_3 \boldsymbol{x}_v + \gamma_3 \boldsymbol{N} &= 0 \end{aligned} \tag{13}$$

Where the coefficients $\alpha_i, \beta_i, \gamma_i,\ i = 1, 2, 3$ are functions of E, F, G, e, f, g. Since $\boldsymbol{x}_u, \boldsymbol{x}_v, \boldsymbol{N}$ are linearly independant, each coefficient is zero, thus we have nine relations:

$$\alpha_i = 0 \quad \beta_i = 0 \quad \gamma_i = 0 \qquad i = 1, 2, 3$$

The relation $\beta_1 = 0$ is the equation

$$\begin{aligned} (\Gamma^2_{12})_u - (\Gamma^2_{11})_v + \Gamma^1_{12}\Gamma^2_{11} + \Gamma^2_{12}\Gamma^2_{12} - \Gamma^2_{11}\Gamma^2_{22} &= -E\frac{eg - f^2}{EG - F^2} \\ &= -EK \end{aligned} \tag{14}$$

This formula is called the Gauss formula. Earlier, we proved the Christoffel symbols may all be expressed in terms of the I-form. Using this fact, and the above equation, we have an expression for the Gaussian curvature K which respects only the first fundamental form. Thus we know Gaussian curvature is an *intrinsic* property of a surface, and thus invariant under local isometries.

Theorem 5 (The Remarkable Theorem)**.** *The Gaussian Curvature K is determined solely by the First Fundamental Form and thus is invariant under local isometry. The equation relating K and I is called the Gauss Formula.*

Compatibility Two other important equations are obtainable in much the same manner as the Gauss Formula. They are called the Codazzi-Mainardi equations and together with the Gauss Formula they are called the *compatibility equations.*

Of the nine relations implied by 13 we only used one, $\beta_1 = 0$, to find the Gauss formula. Analyzing the rest of these equations, we find that $\alpha_1 = 0$, $\alpha_2 = 0$ and $\beta_2 = 0$ all produce equivalent versions of the Gauss formula. We also find $\gamma_3 = 0$ is an identity. The remaining relations, $\gamma_1 = 0$,$\gamma_2 = 0$,$\alpha_3 = 0$ and $\beta_3 = 0$ between them produce two unique relations:

$$\begin{aligned} e_v - f_u &= e\Gamma^1_{12} + f(\Gamma^2_{12} - \Gamma^1_{11}) - g\Gamma^2_{11} \\ f_v - g_u &= e\Gamma^1_{22} + f(\Gamma^2_{22} - \Gamma^1_{12}) - g\Gamma^2_{12} \end{aligned} \tag{15}$$

These are called the Codazzi-Mainardi equations.

The Bonnet Theorem This result is paramount.

Theorem 6 (Fundamental Theorem of Surfaces)**.** *Letting E, F, G, e, f, g be functions subject to the following specifications*

1. *all are differentiable*
2. *all are defined on an open patch* $W \subset \mathbb{R}^2$
3. $E, G, EG - F^2 > 0$
4. *they collectively satisfy the Gauss-Codazzi-Mainardi system*

then you have $\forall p \in W$, $\exists$ *a neighborhood* $U \subset W$ *of* p *and a diffeomorphism* $\boldsymbol{X} : U \to \boldsymbol{x}(U) \subset \mathbb{R}^3$ *s.t.* $\boldsymbol{x}(U)$ *is a regular surface with functions E, F, G, e, f, g as the coefficients of its fundamental forms. Moreover, this diffeomorphism is unique up to rigid motion in* $\mathbb{R}^3$*. Such a diffeomorphism is called an immersion.*

This adds up to a geometric explanation for those mysterious compatibility functions. If we think of the first and second fundamental form as matrices of functions over local surfaces instead of matrices of scalars at point, then for arbitrary choices of a I-form and a II-form the compatibility equations specify whether there exists a surface in $\mathbb{R}^3$ with said forms. Our notion of existence here allows for S to intersect with itself. Immersions which do not admit self-intersections are called embeddings.

2 Approaching the Problem

Recall the problem: we want to "embed" a surface in a ball, $B_0(1) \subset \mathbb{R}^3$ such that the surface is everywhere negatively curved. With more precision, we want to prove there are compatible I and II forms which correspond to a surface of everywhere negative curvature, and for which there exists a diffeomorphism $\boldsymbol{x} : U \subset \mathbb{R}^2 \to \boldsymbol{x}(U) \subset \mathbb{R}^3$ satisfying the conditions $\boldsymbol{x}(U) \subseteq B_0(1)$ and $\boldsymbol{x}(U)$ is a regular complete surface without self-intersection.

2.1 A Perfunctory Sketch of a Solved Embedding Problem

For clarity's sake I will make a sketch of a solution to an arbitrary embedding problem.

Suppose I want to find an embedded surface with some arbitrary curvature specification. The first step amounts to finding a metric or metrics associated with desirable curvatures. The metric is all we need to specify curvature per the Remarkable Theorem. Then, I find a "compatible" II-form by solving the compatibility system. Now I apply Bonnet's theorem and I know there exists a diffeormorphism which is an immersion into $\mathbb{R}^3$. All that's left is to prove the diffeomorphism obtained by Bonnet's theorem does not self intersect. Thus we have an embedding, and the surface hunt is over. Bare bones, we have:

1. Start: "I want an embedded surface of given curvature"
2. (uses Gauss Formula) "I have a metric producing the desired K"
3. (solves G-C-M Compatibility eq.) "I have a II-form compatible with my metric"
4. (uses Bonnet's Theorem) "I have an immersion of a surface with the desired K"
5. (proves no self intersection) "I have found an embedded surface with the desired K"

2.2 Our Embedding Problem

Like the generic problem above, we are searching for an embedded surface with a specification on K. We have other specifications on our surface as well. In total, they are:

1. The Gaussian Curvature K is strictly negative at all points.
2. The surface is bounded in $\mathbb{R}^3$, i.e we can scale it to fit in the unit ball.
3. The surface is embedded (it does not intersect itself).
4. The surface is "nice" everywhere. (i.e. complete, smooth and regular).

"Wait. That Can Exist?" It can (hopefully), but only in a certain sense. The conventional wisdom is that any bounded surface must in some instant intersect for the first time with a plane drawn from infinity. If we additionally specify completeness and smoothness, then at any point p where intersection first occurs, in all directions the surface either curves away from the the tangent space or stays in the tangent space. I.e. the surface has non-negative curvature at this point.

There is a way around this problem. Remove the the set of points which first intersect planes from infinitity, leaving open boundaries behind. Extrinsically, the surface is no longer complete. However, it may still be intrinsically complete if the incomplete points are an infinite distance away from all the other points.

This tells us that the best we are going to get in terms of completeness is intrinsic completeness.

Remark 3. Without further developments, our solution prospects would be rather bleak. However, a clever construction of Rozendorn's allows us to reduce the problem and remarkably improve our chances at a solution.

3 Rozendorn's Surface

Rozendorn has constructed an embeddable, one parameter family of bounded, intrinsically complete surfaces, with everywhere nonpositive curvature. We can use the existence of this family to our advantage, as you will see. For now, we survey the construction.

3.1 Construction of Rozendorn's Surface

Rozendorn constructs his surface by developing an infinite set of tinkertoy-like building blocks which he then glues together along their boundaries. The manner in which he does this takes advantage of the variance in limiting behavior between intrinsic and extrinsic distances.

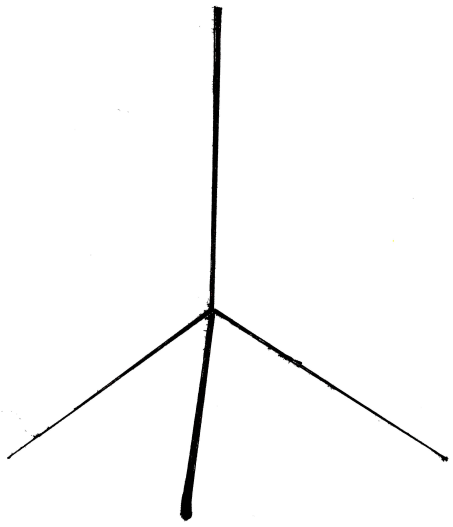

Figure 3: Tripod

"Tinker Toys" The above tripod figure is where Rozendorn's tinkertoys begin their life. Rozendorn develops them by a thickening procedure where the parameter over which the family of surfaces varies is the scale of the thickening relative to the absolute size of the tinker toys.

This object has negative curvature everywhere except at four monkey saddle points. These points are located in the center of each "face" of the tinkertoy corresponding to each face of the overlaid tetrahedron. Starting with a single S_4 symmetric tinkertoy we begin a gluing procedure that attaches another tinker toy to each open end of the first along respective boundary elements [5].

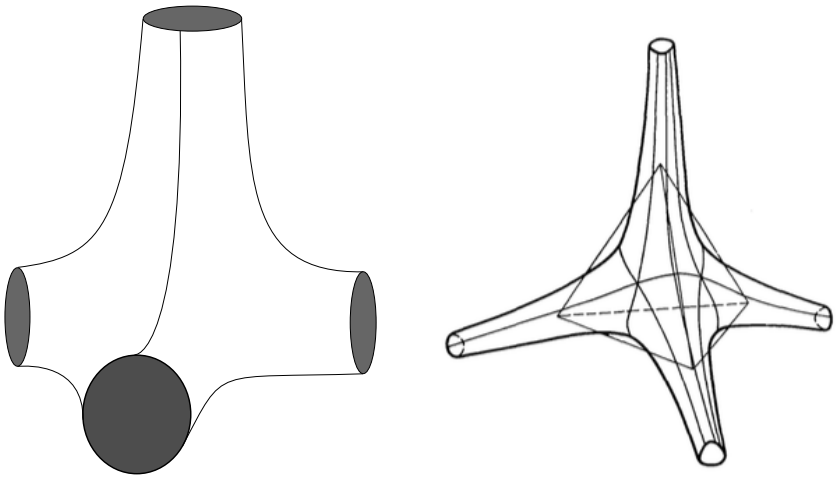

(a) Fattened Tripod

(b) Fattened tripod overlaid with a tetrahedron.

Figure 4: Two images of Rozendorn's Tinkertoys

The dimensions change across generations; extremal tinkertoys have smaller symmetric groups because their open "branch" ends are smaller than the "trunk" end. This change scales with generation.

The gluing is done so that distinct generations are contained in disjoint concentric shells, the outer radii of which increase proportionally to

$$\sum_{i=1}^{n} \frac{1}{i^2}$$

where n is the generation of the shell. This guarantees boundedness, as $\sum_{i=1}^{\infty} \frac{1}{i^2}$ converges.

Completeness Simply gluing on an infinite number of‘ tinkertoys won't ever compactify the surface, so to obtain intrinsic completeness Rozendorn employs the following beautiful argument. On any pair of concentric spherical shells there is a relation between the ratio of radii and the maximum length of line segments contained in the shell.

Calculating this reveals that concentric spherical shells with a radial quotient on the order of

$$\frac{R_n}{R_{n-1}} = \frac{\sum_{i=1}^{n} \frac{1}{i^2}}{\sum_{i=1}^{n-1} \frac{1}{i^2}}$$

contain a tangent vector of maxium length on the order $\frac{1}{n}$ [6].

Rozendorn manages to show that he is free to choose tinkertoy dimensions s.t. the surface curve paths from the center out to the nth spherical shell have

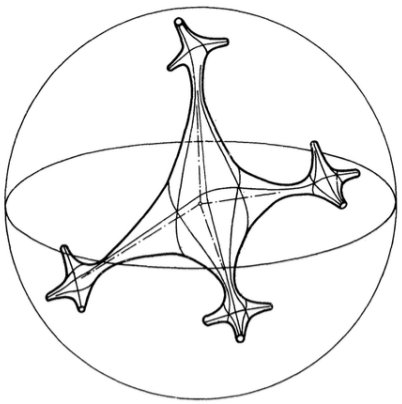

Figure 5: The first and second generation tinkertoys glued together.

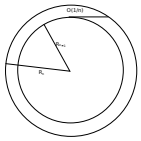

Figure 6: A cross section of concentric spherical shells with radii R_n, R_{n-1}, and maximum length tangent ray.

limiting behavior qualitatively identical to the sum of these tangent line lengths. The sum of tangent line lengths is

$$\sum_{i=1}^{n} \frac{1}{i}$$

This sum is divergent. Thus, the distance from any point on the surface to the "end" of the surface is infinite, thus the surface is intrinsically complete.

4 What's Rozendorn to Us?

The embeddibility of Rozendorn's surface implies its I and II forms are a solution to the compatibility system. Since it is negatively curved except on a countable set, Rozendorn's surface is the surface we want nearly everywhere. This means if we choose a subset of Rozendorn's surface containing all of its $K = 0$ points, and solve the embeddibility problem along this much simpler set, then we get the rest of the embedding for free. We attempt this with a reduction to patches.

4.1 A "Patchy" Deformation

So consider a patch $V : [0,1] \to S$ on Rozendorn's surface of arbitrary size, containing a single K=0 point. Let $I_0[u,v]$ and $II_0[u,v]$ be the fundamental forms of Rozendorn's surface, as functions in intrinsic coordinates. We cannot perturb away the zero point, so we will "push" the zero-curvature points to the infinitely far away boundary, intrinsically removing them from the surface.

To accomplish this, we attempt to construct an iterative patching method. It should go something like this: Let V be the patch defined above, and let $I[u,v,t]$ and $II[u,v,t]$ be the fundamental forms on the patch where t=0 corresponds to the Rozendorn surface and the parameter t $\in [0,1]$ tracks the progress of the deformation. Specify $\forall\, t \in [0,1]$ and $\forall\, (u_0, v_0) \in \partial V$ that

$$\begin{aligned} I_0[u_0,v_0] &= I_t[u_0,v_0] \\ II_0[u_0,v_0] &= II_t[u_0,v_0] \end{aligned} \tag{16}$$

This condition fixes the boundary of V, thus keeping it in agreement with the rest of Rozendorn's surface. Now, we construct this deformation so that the compatibility equations stay satisfied, and analyze the resultant constraints on the fundamental forms. That analysis will tell us whether or not we may choose a metric on V s.t. the $K = 0$ point moves up the surface.

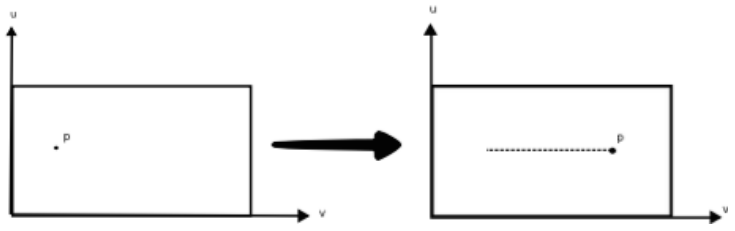

Figure 7:

Supposing we can choose such a metric, we then iterate this procedure by choosing a new patch further out on the surface which contains the same zero point, but in its new location, and pushes it using the same technique. This is possible because we are always able to pick a patch whose local geometry is identical to the original patch's local geometry. Why this is true is described in the following section.

5 Topological Hurdles

A major obstacle to removing these critical points is the topological constraint described by the Poincaré-Hopf Theorem. To introduce this theorem's role in our problem, we must first introduce the notion of asymptotic line curves.

5.1 Asymptotic Line Fields

All negatively curved surfaces admit line fields obtainable from the II-form.

Definition 8 (Asymptotic Directions)**.** let S be an everywhere negatively curved surface with a point p. Let

$$\begin{bmatrix} e & f \\ f & g \end{bmatrix}$$

be the II-form of S at p. Then vectors $w, r \in T_p(S)$, in intrinsic coordinates, point in asymptotic directions if

$$w^t \begin{bmatrix} e & f \\ f & g \end{bmatrix} w = r^t \begin{bmatrix} e & f \\ f & g \end{bmatrix} r = 0$$

At each point there are two solutions, which respectively correspond to two families of lines on the surface. These form line fields on the surface which correspond to each other and the principle curvature directions in the following way: at any paticular point, the angle bisectors of the two asymptotic directions are the principle curvature directions of the surface at said point.

On the Rozendorn surface, the asymptotic line fields look like this

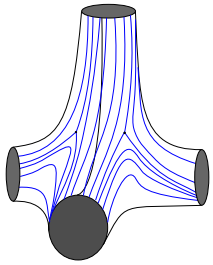

Figure 8: The center Tinkertoy with asymptotic lines drawn in blue.

5.2 Poincaré-Hopf Theorem

Theorem 7 (Poincaré-Hopf)**.** *Let $S \in \mathbb{R}^3$ be a surface, L a line field on S and x_i, $i = 1, 2, 3...$ be a countable number of critical points. Then*

$$\sum_i Index_{x_i}(L) = \chi(S)$$

To make sense of this we must define the "index" of a critical point.

Definition 9 (index)**.** Let S be a surface, L be a line field on S, and $p \in S$ be a point on S at which there is a critical point of L. Then consider the set $D_p(\epsilon) = B_p(\epsilon) \cap S$ s.t. $\epsilon > 0$ is small enough to exclude any other critical points. Then the degree of the Gauss map along $\partial D_p(\epsilon)$ is called the index of the critical point at p.

We can more easily calculate around the index of a critical point by drawing the asymptotic line field on $\partial D_p(\epsilon)$ and counting the number of times it "turns". For example:

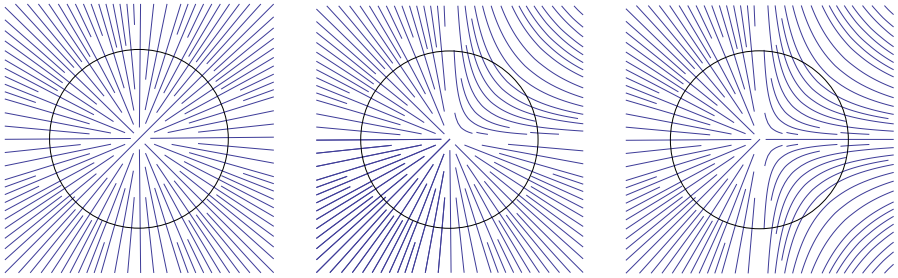

(a) Index=1 (b) Index=$\frac{1}{2}$ (c) Index=0

Figure 9: These depict the disk boundary $\partial D_p(\epsilon)$, and the asymptotic line field.

it is important to note that a turn contributes negative values to the index if it turns in the direction opposite the orientation of $\partial D_p(\epsilon)$. Thus,

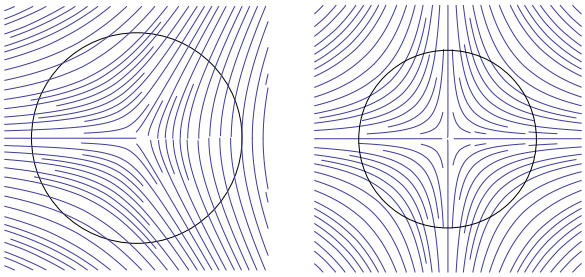

(a) Index=$-\frac{1}{2}$ (b) Index=-1

Figure 10: Boundary elements with negative index.

5.3 Index Manipulations

We now show we can push the critical points to the boundary without violating the Poincaré-Hopf theorem. To achieve this, we topologically evaluate individual tinkertoys in a quasi-inductive fashion.

First Generation To start, we illustrate the center toy, pre-deformation.

For all index calculations, we treat a toy as a sphere where our boundaries correspond to some $\partial D_p(\epsilon)$ for a virtual critical point p outside the toy. For this particular toy we have,

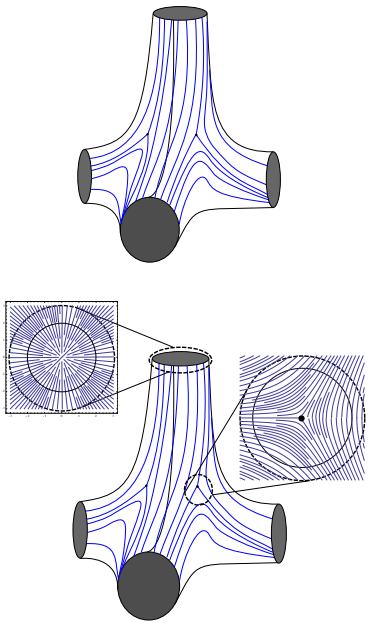

Figure 11: Critical Indices on a Tinkertoy

Thus

$$Index_{boundary} = 1 \qquad Index_{K=0point} = -\frac{1}{2}$$

$$\sum_i Index_{x_i} = 4(1) + 4(-\frac{1}{2}) = 2 = \chi(S^2)$$

Now we draw each critical point through an adjacent neck, such that no two points leave through the same neck $[fig : 12]$.

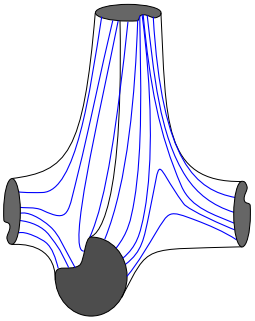

Figure 12: The deformed first generation toy

At each boundary the line field looks like figure $9(b)$. Thus the index contri-

bution of each end is $\frac{1}{2}$ and

$$\sum_i Index_{x_i} = 4(\frac{1}{2}) = 2 = \chi(S^2)$$

satisfying the Poincaré-Hopf theorem.

Second Generation Every tinker toy in the second generation recieves a single critical point along the "trunk". This critical point is naturally matched to native critical point on the second generation toy by the asymptotic line fields [13].

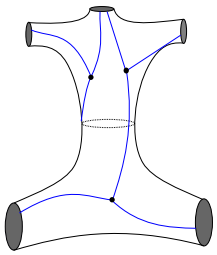

Figure 13: Asymtotic lines (in blue) connect pairs of points across tinkertoy trunks

Proceeding, we drag the non-native critical point behind this matched native critical point through one of two branches adjacent to the native critical point. This leaves behind 3 points and two unaffected branches. One of the remaining

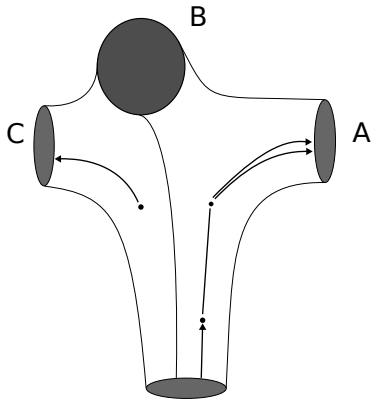

Figure 14:

three points will be pushed, alone, through an available neighboring branch, just as was done in the first generation. This point should be adjacent to the trunk boundary. Now there are two points and only one remaining branch. One

of these two is adjacent to the trunk boundary. We push this point along a principle curvature direction towards the other. Then, we push both of them through the unused branch. Now we evaluate the index contributions of each

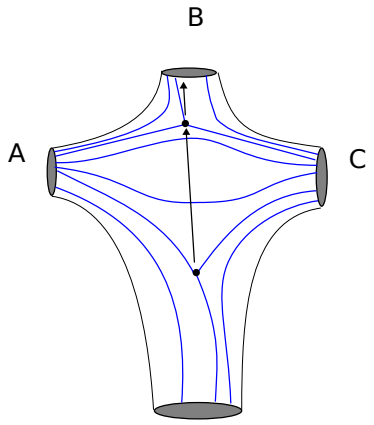

Figure 15:

boundary element to check against the Euler characteristic.

1. Branch A has accepted two critical points across its boundary. The resulting asymptotic line field along the boundary is identical to Figure 9(c), thus
$$Index_A = 0$$

2. Branch B appears different from A. Now, the two points are not "connected" as they were in A. However, the interstital behavior and the index is identical to branch A.
$$Index_B = 0$$

3. Branch C is identical to the branches of the first generation, thus we know
$$Index_C = \frac{1}{2}$$

4. The asymptotic line field around the trunk is the inversion of the line field on the first generation boundary the trunk was glued to. This has the following effect:
$$Index_{trunk} = \chi(S^2) - Index_C = 2 - Index_C = \frac{3}{2}$$

Thus we have
$$\sum_{x_i} Index_{x_i} = 2(0) + \frac{1}{2} + \frac{3}{2} = 2$$

We should explain the result for the trunk boundary. Remember when we calculate the index contribution of a boundary element ∂D, we are imagining there is a disk, D, containing a virtual critical point, p, such that D completes the figure along ∂D and the index of the virtual critical point p is identically the index contribution of ∂D.

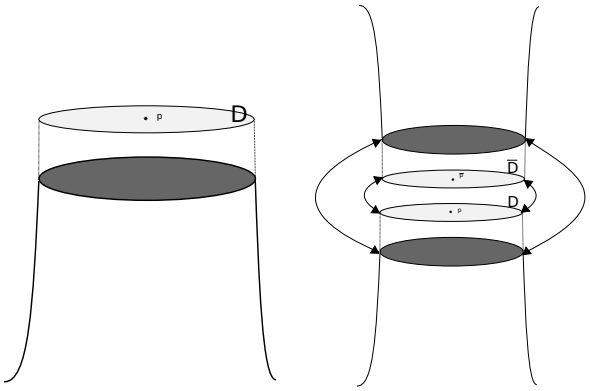

(a) The "virtual" critical point p and it's home disk D

(b) Gluing p and D to $\overline{p}$ and $\overline{D}$

Figure 16:

Now consider a new figure having an identical boundary element $\overline{\partial D}$ and calculate the index contribution of $\overline{\partial D}$ to the new figure. Again, we imagine a disk $\overline{D}$ containing a critical point, $\overline{p}$, such that $\overline{D}$ completes the new figure along $\overline{\partial D}$ and the index of $\overline{p}$ is identically the index contribution of $\overline{\partial D}$. Now we see the crux: If we glue together the old and new figures along the boundary element ∂D and $\overline{\partial D}$ [16(b)], then we also glue together the imaginary disks, D and $\overline{D}$. Since these disks contain critical points p and $\overline{p}$, and together will form a 2-sphere, we have

$$Index_p + Index_{\overline{p}} = \chi(S^2) = 2$$

Since we identify the index contribution of $\overline{p}$ and ∂D on the new figure, we have

$$Index_{\overline{\partial D}} = \chi(S^2) - Index_{\partial D} = 2 - Index_{\partial D}$$

Generalization In subsequent generations, the toys become increasingly diverse, so a generational treatment is ugly. Instead, we reclassify every tinkertoy by the index of their trunk boundary, and induct over this index. We see this is the right thing to do by generalizing the pattern from the second generation.

The second generation toys' critical point pairs which crossed branches A and B behave identically thereon: the leading non-native critical point collects

a new, native critical point it is matched with. Then the resulting order three critical point bundle crosses an adjacent boundary element into the fourth generation toys. The remaining three native critical points and two branches are treated identically as in generation two. Thus we see although there are two methods of generating an order two critical point bundle, the treatment thereafter is identical. Moreover, this method of critical bundles "collecting" the matched point and moving on shows every tinkertoy on Rozendorn's surface can be treated identically up to the order of the critical point bundle. Since the order of the incident critical point bundle determines the index of the trunk boundary, classifying tinkertoys by trunk index makes sense.

Theorem 8. *Given an arbitrary tinkertoy which has accepted a critical point bundle of order n, the index of the trunk boundary element can be written*

$$1 + \frac{1}{2}n$$

Proof. Recall that given a trunk boundary element $\overline{\partial D}$ glued to a branch boundary element ∂D we have

$$Index_{\overline{\partial D}} = \chi(S^2) - Index_{\partial D} = 2 - Index_{\partial D}$$

If we send a critical bundle of order n across ∂D, the asymptotic line field will contain the wake of each point. Each wake corresponds to negative half turn in the asymptotic line field, thus we can write

$$Index_{\partial D} = 1 - \frac{1}{2}n$$

Immediately producing the desired result

$$Index_{\overline{\partial D}} = 2 - Index_{\partial D} = 1 + \frac{1}{2}n$$

□

Example 1. Consider the second generation tinkertoys. They accept an order n=1 critical point, thus they have a trunk index $1 + \frac{1}{2}n = \frac{3}{2}$

Finally we can perform our quasi-induction. We consider a tinkertoy which accepts a critical point bundle of arbitrary order n, thus in the class of tinkertoys with trunk index $1 + \frac{1}{2}n$. As before, the leading point in the critical point bundle is naturally matched via the asymtotic lines to a native critical point. The critical point "collects" this new point, thus becoming of size n+1, and exits through an adjacent boundary element A. The remaining three critical points, and two branches are treated identically to generation two. The index contribution of A can be calculated using the formula in the above proof:

$$Index_A = 1 - \frac{1}{2}(n+1) = 1 - \frac{1}{2} - \frac{1}{2}n$$

using n+1 because the bundle has acquired the native point. Thus we have

$$Index_A + Index_{trunk} = \frac{3}{2}$$

This is an identical result to generation two. Since the other two boundaries are also identical to the generation two solution we have a solution for abitrary trunk index and thus for the whole surface.Fig

Pushing Bundles The previous work makes a great use of our ability to push bundles of critical points along the surface. However, when describing the patch embedding problem in a previous section, we specified each patch to contain exactly one critical point; our solution was not generalized to arbitrary order bundles. To do this, we push the leading point forward some arbitrary distance, thus giving us space to push the second in line and so on.

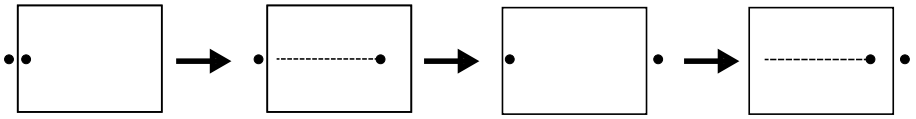

Figure 17: How to push an order 2 point bundle

Notably, the asymptotic line fields around a particular zero point do not qualitativly change as we iterate the patch deformations. This means the local geometry of the zero points do not change, and thus the arbitrary patch solution is iterable.

6 A Single Patch

Finally, we attack the single patch deformation problem. The following section consists of approaches used and the various results produced. All methods make use of a conformal choice of intrinsic coordinates to simplify the calculations. This technique is developed in the following subsection.

6.1 Conformal Coordinates

Earlier, we proved the following relation: given a surface S and a parameterization $\boldsymbol{X} : \mathbf{U} \subset \mathbb{R}^2 \to \mathbb{R}^3$ such that $\boldsymbol{X}(\mathbf{U}) = S$, we can write the first fundamental form of S as the matrix

$$I = \begin{bmatrix} E & F \\ F & G \end{bmatrix} = \begin{bmatrix} \langle \boldsymbol{x}_u, \boldsymbol{x}_u \rangle & \langle \boldsymbol{x}_u, \boldsymbol{x}_v \rangle \\ \langle \boldsymbol{x}_v, \boldsymbol{x}_u \rangle & \langle \boldsymbol{x}_v, \boldsymbol{x}_v \rangle \end{bmatrix}$$

So the first fundamental form can be thought of as a function of the parameterization. With this in mind, we recall that a surface can be equivalently

parameterized in many ways, more if we're using the intrinsic notion of equivalence. Then, we see the possible expressions for the I-form of a given surface form a corresponding equivalence class in the 2x2 symmetric matrices.

This business of conformal coordinates amounts to a special case of the above fact. Our freedom to choose a coordinate basis for the patch $\mathbf{U} \subset \mathbb{R}^2$ tells us the above equivalence class is at least as big as the class of similar matrices. Furthermore, the I-form's symmetry implies it is similar to a diagonal matrix. Thus we always have a choice of coordinates that diagonalizes the I-form locally, i.e F=0. More than this, the I-form is positive definite, allowing us to then scale the diagonalizing coordinate choice to force E=G.

6.2 Direct Manipulation

We first consider a patch $V[0,1] \to S$ on Rozendorn's surface, with a conformal choice of coordinates. The conformal I-form on V

$$I_0(u,v) = \begin{bmatrix} E_0(u,v) & 0 \\ 0 & G_0(u,v) \end{bmatrix} \quad s.t. \quad E_0(u,v) = G_0(u,v)$$

is positive definite; thus

$$\exists\, \lambda_0(u,v)\; s.t.\; E_0(u,v) = G_0(u,v) = e^{2\lambda_0(u,v)}$$

We want the deformation to be smooth, and thus trackable by a continuous parameter $t \in [0,1]$. Clearly the patch's I-form will depend on t, so we write

$$I(u,v,t) = \begin{bmatrix} e^{2\lambda(u,v,t)} & 0 \\ 0 & e^{2\lambda(u,v,t)} \end{bmatrix}$$

where $\lambda_0(u,v) = \lambda(u,v,0)$.

Similarly, we write the second fundamental form as a function in u,v and t.

$$II = \begin{bmatrix} L(u,v,t) & M(u,v,t) \\ M(u,v,t) & N(u,v,t) \end{bmatrix}$$

Using L,M and N instead of e,f and g to avoid confusion with the number e. As before, the parameter t tracks the deformation, i.e.

$$II_0 = \begin{bmatrix} L(u,v,0) & M(u,v,0) \\ M(u,v,0) & N(u,v,0) \end{bmatrix}$$

is the II-form on Rozendorn's original surface. We write the Codazzi-Mainardi system in terms of the functions L,M, and N.

$$\begin{aligned} L_v - M_u &= L\Gamma^1_{12} + M(\Gamma^2_{12} - \Gamma^1_{11}) - N\Gamma^2_{11} \\ M_v - N_u &= L\Gamma^1_{22} + M(\Gamma^2_{22} - \Gamma^1_{12}) - N\Gamma^2_{12} \end{aligned} \tag{17}$$

Recalling the Christoffel symbols are expressable in terms of the entries of the I-form, we make the appropriate substitutions. This produces the system

$$\begin{aligned} L_v - M_u &= L\frac{1}{2}\frac{E_v}{E} + M(\frac{1}{2}\frac{G_u}{G} - \frac{1}{2}\frac{E_u}{E}) + N\frac{1}{2}\frac{E_v}{G} \\ M_v - N_u &= -L\frac{1}{2}\frac{G_u}{E} + M(\frac{1}{2}\frac{G_v}{G} - \frac{1}{2}\frac{E_v}{E}) - N\frac{1}{2}\frac{G_u}{G} \end{aligned} \tag{18}$$

Now we make use of the conformal choice of coordinates, rewriting the above system in terms of the function $\lambda[u, v, t]$.

$$\begin{aligned} L_v - M_u &= (L+N)\lambda_v(u,v,t) \\ N_u + M_v &= (L+N)\lambda_u(u,v,t) \end{aligned} \tag{19}$$

Given $\lambda(u, v, t)$ is Lipschitz continuous, we can produce the integral equation:

$$\lambda(u,v,t) = A(u,t) + \int_0^v \frac{L_v(u,s,t) - M_u(u,s)}{L(u,s) + N(u,s,t)}\, ds \tag{20}$$

Where A(u,t) is an arbitrary function in u corresponding to the u dependent terms of $\lambda(u, v, t)$. Substituting the above expression for $\lambda(u, v, t)$ into the second Codazzi-Mainardi equation produces the relation

$$\int_0^v \frac{(L_{uv} - M_{uu})(L+N) - (L_v - M_u)(L_u + N_u)}{(L+N)^2}\, ds + A_u(u,t) = \frac{N_u - M_v}{L+N} \tag{21}$$

Let the derivative $A_u(u, t)$ be represented by an arbitrary function in u and t, $f(u, t)$, and we have a constant C such that

$$A(u,t) = C + \int_0^u f(w,t)dw \tag{22}$$

Substituing $f(u, t)$ for $A_u(u, t)$ in [21], we get the relation:

$$f(u,t) = \frac{N_u - M_v}{L+N} - \int_0^v \frac{(L_{uv} - M_{uu})(L+N) - (L_v - M_u)(L_u + N_u)}{(L+N)^2}\, ds$$

and because f is independent of v, we let v=0 and see

$$f(u,t) = \frac{N_u(u,0,t) - M_v(u,0,t)}{L(u,0,t) + N(u,0,t)}$$

Applying this result to [22] and the subsequent result to [20] we produce the following equation.

$$\lambda(u,v,t) = C + \int_0^u \frac{N_u(w,0,t) - M_v(w,0,t)}{L(w,0,t) + N(w,0,t)} dw + \int_0^v \frac{L_v(w,s,t) - M_w(w,s)}{L(w,s) + N(w,s,t)}\, ds \tag{23}$$

Where $\forall\, t \in [0,1], \quad C = \lambda(0,0,t) \quad and \quad A(u,t) = \lambda(u,0,t)$. Notably, this demands mixed partial equality from $\lambda(u, v, t)$. To summarize, a conformal/isothermal metric with a function $\lambda = \frac{1}{2}ln(E) = \frac{1}{2}ln(G)$ such that λ is at least C^2 differentiable, and solves equation [23] must satisfy the Codazzi-Mainardi equations.

Now, we will introduce constraints on $\lambda(u, v, t)$ so that any solution satisfying all constraints would correspond to a metric with the desired qualities. To start, we want for any $(u_0, v_0) \in \partial V$, and $\forall t \in [0, 1]$,

$$\begin{aligned} \lambda(u_0, v_0, t) &= \lambda(u_0, v_0, 0) \\ II(u_0, v_0, t) &= II(u_0, v_0, 0) \end{aligned} \tag{24}$$

i.e. the deformation maintains the boundary values for the I and II forms. We also need the point at which $K = 0$ to "move" up the patch. This condition can be written as

$$\int_0^{\frac{2}{3}} e^{2\lambda(u,v,t)} |\lambda(u, v, t)| \, du - B \int_0^{\frac{2}{3}} e^{2\lambda(u,v,0)} |\lambda(u, v, 0)| \, du \geq 0 \tag{25}$$

Where B is some positive constant, and v is fixed. This specifies that the length of the image curve grows by some factor B large enough to diverge as we iterate.

Now we do a funny thing. We introduce a new function, b(u,v,t), defined in relation to the II form by the equation

$$II = e^{b(u,v,t)} \overline{II}$$

with $det[\overline{II}] = 1$. We are pushing a bit of our freedom to choose II into this simpler function b, hoping that b will have enough freedom to guarantee some solution for λ despite the constraints. In general, we proceed as follows

1. We specify the function $\lambda(u, v, t)$ to agree on the boundary v=0 and corresponding to the target patch curvature given by

$$K = \frac{-1}{2e^{2\lambda}} \left(\lambda_{uu} + \lambda_{vv}\right)$$

2. Choose λ to satisfy the length condition 25

3. We pick the function b(u,v,t) so that

$$\int_0^{\epsilon} \partial t \left(\frac{\partial v(b(u, v, t)\overline{L}) - \partial u(b(u, v, t)\overline{M})}{b(u, v, t)(\overline{L} + \overline{N})} \right) dv = 0$$

   thus satisfying the boundary at $v = \epsilon$.

The equation for curvature under item 1 above is equivalent to the Gauss equation for curvature. Thus this method will automatically satisfy the Gauss equation. Furthermore, rexpressing our previous results to contain b(u,v,t) and the entries of $\overline{II}$ is very nice. However, there aren't relevant general existence results for equations like 23, so we considered other methods.

6.3 Rozhdestvinskii-Poznyak Reformulation

We found a useful reformulation of the compatibility equations attributed to Rozhdestvinskii-Pozynak (see [Ve67] and [BVK73]). It starts by scaling the L,M,N functions with respect to the I-form. We let

$$l, m, n = \frac{(L, M, N)}{\sqrt{det[I]}} = \frac{L, M, N}{e^{2\lambda}}$$

which produces a new expression for the compatibility equations.

$$l_v + l\lambda_v = n\lambda_v + 2m\lambda_u + m_u \tag{26}$$

$$m_v + 2m\lambda_v = n_u + (n - l)\lambda_u \tag{27}$$

$$K^2 = m^2 - ln \tag{28}$$

Then we introduce new functions R and S, with

$$S(u, v, t) := \frac{(m - K)}{n} \qquad R(u, v, t) := \frac{-(m + K)}{n}$$

Substituting these into our new compatibility system yields an even newer expression for the compatibility equations.

$$0 = \overrightarrow{w}_u + A\overrightarrow{w}_v + \overrightarrow{B} \tag{29}$$

Where the vectors $\overrightarrow{w}, \overrightarrow{B}$ and the matrix, A, are given below.

$$\overrightarrow{w} = \begin{bmatrix} K(u, v) \\ \lambda(u, v) \end{bmatrix}$$

$$A = \begin{bmatrix} \frac{\left(2S^2+1\right)R^2+S^2}{(R+S)(RS+1)} & \frac{2K\left(R^2+1\right)\left(S^2+1\right)}{(R+S)(RS+1)} \\ -\frac{(R-S)^2}{2K(R+S)(RS+1)} & -\frac{R^2+S^2+2}{(R+S)(RS+1)} \end{bmatrix}$$

$$B = \begin{bmatrix} \frac{2K\left(R\left(R_v\left(-\left(S^3+S\right)\right)-R_u\left(S^2+1\right)+\left(R^2+1\right)SS_v\right)+\left(R^2+1\right)SS_u\right)}{(R-S)(R+S)(RS+1)} \\ \\ \frac{R_vS+R_u+RS_v+S_u}{(R+S)(RS+1)} \end{bmatrix}$$

Although this formulation is not simpler, the form of equation 29 allows us to use the method of characteristics, a powerful method of solving PDE.

6.4 Method of Characteristic Curves for PDE

The big idea behind the method of characteristics is that for a PDE on some domain there is a family of curves in the domain along which the PDE reduces to an ODE.

Starting with our equation

$$0 = \overrightarrow{w}_u + A\overrightarrow{w}_v + \overrightarrow{B}$$

we introduce an arbitrary curve, α parameterized in s: $\alpha(s) = (u(s), v(s))$. We want to solve for the function $\overrightarrow{w}$ in terms of the R and S functions. We can write the function $\overrightarrow{w}$ along $\alpha(s)$ as

$$\overrightarrow{w} = \begin{bmatrix} K(u(s), v(s)) \\ \lambda(u(s), v(s)) \end{bmatrix}$$

and subsequently differentiate in s to produce the relation

$$\overrightarrow{w}_s(u(s), v(s)) = u'(s)\overrightarrow{w}_u + v'(s)\overrightarrow{w}_v$$

If we let

$$\begin{aligned} u'(s) &= 1 \\ v'(s) &= A \end{aligned} \tag{30}$$

then for any solutions $\overrightarrow{w}$ on the characteristic curves defined by 30

$$\overrightarrow{w}_s = -B \tag{31}$$

In other words, the curve $\phi : [0, 1] \to \mathbb{R}^4$ such that $\phi(s) = (u(s), v(s), K(u(s), v(s)), \lambda(u(s), v(s)))$ has derivative

$$\frac{d}{ds}\phi(s) = \begin{bmatrix} u(s) \\ v(s) \\ K(u(s), v(s)) \\ \lambda(u(s), v(s)) \end{bmatrix} = \begin{bmatrix} 1 \\ A \\ -B \end{bmatrix}$$

Defining the "Characteristic Vector Field" for the system. Given some initial data, the union of integral curves of this vector field form a solution to the PDE.

For us, the difficulty lies in that we are specifying a complete boundary, not just an initial value line. We have solutions for the characteristic curves of the system, so the problem now amounts to proving the set of solutions for $\overrightarrow{w}$ contains elements which both match up with our boundary conditions and satisfy the curvature and distance constraints. This is equivalent to showing we have enough freedom to choose functions R and S which fix the boundary and determine $\lambda(u, v)$ favorably.

7 A Related Problem

The reason we reduced our global embedding problem to a patch embedding problem is, of course, to simplify the problem at hand. However, this reduction has the extra effect of generalizing our result. By that, I mean if we were to solve the embedding problem on the Rozendorn patch, then our result would be valid for other nonpositively curved surfaces with isolated umbilical points!

Cool. So? Well, you probably know there are a lot of strictly negatively curved surfaces out there, but there is only one with just cusp ends. This is Vaigant's surface [BZ92]. There's likely more that we don't know of yet,

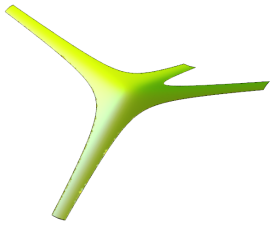

Figure 18: Vaigant's surface

so discovering these kinds of surfaces is nontrivial result. The generality of our patch embedding method lets us take surfaces, like Rozendorn's tinkertoys, which are negatively curved except on a countable number of isolated umbilical points, stretch their boundaries out to infinity (thus giving them cusp ends), and then intrinsically remove their umbilical points. The result is a strictly negatively curved surface with only cusp ends.

"But WAIT! There's more." An interesting question to ask about these kinds of surfaces is can they have an arbitrary genus? This is non-trivial because maybe for some obscure reason a genus five (or two or 17) surface can never have cusp ends and be negatively curved. This question is answered very quickly because we can do the obvious thing and build tori with of Rozendorn's tinker toys.

If we get four of those nice looking, symmetric, first generation tinker toys, we can build a punctured torus. We glue each tinker toy to two others forming a ring with eight open tubes. We then extend the tubes to infinity, remove the zero points and we have a strictly negatively curved surface with only cusp ends and genus 1. This process is clearly extendable; two more tinkertoys glued in the right place adds another handle to our figure, increasing the genus by 1 and so on.

It gets even better. There is a tinkertoy similar to the Rozendorn tinkertoy, but it has six ends instead of four. If I were to construct a surface in the manner previously described, but using one of these six ended doodads in place of a Rozendorn tinkertoy, the swap would not affect the genus of the resulting surface, but would increase the number of ends by two. In fact, if we specify these constructions make chains like FIG, we can choose any number of ends

from the set $n \in \mathbb{N}\, s.t.\, 4(g+1) \leq n \leq 8(g+1)$. More complicated orientations, such as cubical lattices, allow for other numbers of cusp ends.

References

[BVK73] I. Ya. Bakel'man, A. L. Verner, B. E. Kantor, *Introduction to Differential Geometry in the Large*, Nauka, Moscow, 1973, Zbl.276.53093.

[doC76] M. do Carmo, *Differential Geometry of Curves and Surfaces*, (1976)

[Ro66] È. R. Rozendorn, *Weakly irregular surfaces of negative curvature*, Uspehi Mat. Nauk 21 (1966), no. 5 (131), 97-100; English transl. in Russian Math Surveys 21 (1966)

[BZ92] Yu. D. Burago, V. A. Zalgaller, eds, *Encyclopedia of Mathematical Sciences Vol. 48*, Springer-Verlag, New York, 1992.

[Ve67] A. L. Verner, *On the extrinsic geometry of elementary complete surfaces with nonpositive curvature. I*, Mat. Sb. (N.S.) **74** (**116**) (1967), 205-224.

Theorem[section] [theorem]Lemma [theorem]Definition

Classification of Pillowcase Covers

Sarah Butchko
Advisor: Professor Kevin Pilgrim, Indiana University Bloomington

Abstract

We begin with a surface obtained by gluing two squares together. One square is white and labeled with a Q, the other is black and has the reflection of Q as a label, which we will call Q-bar, $\bar{Q}$. This surface Z is called the square pillowcase and is homeomorphic to the sphere.We then can examine branched covering spaces of the square pillowcase, which are the gluing X of several white and black squares such that each white edge is paired with exactly one black edge. The covering map $f : X \longrightarrow Z$ from a pillowcase cover to the square pillowcase is done in the obvious way by sending white squares in the cover to the white square labeled Q in the square pillowcase, similarly for the black squares.This research project involves the classification of such pillowcase covers $f : X \longrightarrow Z$. Classification can be determined in an algebraic way by using permutations that represent each pillowcase cover. This is inherently an idea of sameness between some pillowcase covers and thus we can find equivalence classes in both a visual representation as well as an algebraic process.

1 Preliminaries

1.1 Motivation

Similar research of different surfaces has been previously done, motivating our study of the square pillowcase. Some methods used in this research were adapted from the work of two former Indiana University Bloomington REU students studying the punctured torus, since the torus has many similarities with the square pillowcase. The method for coding and classifying pillowcase covers by use of permutations was inspired by the work of Kathleen Moriarty in her paper on Covering Spaces of the Punctured Torus.[1] The work of Naomi Utgoff looking at affine diffeomorphisms of the torus was useful when in our study of affine transformation of the square pillowcase and its effect on codes. [2]. The work of G. Shmithusen on finding an algorithm for the Veech group of an origami also motivated this study. [3]

1.2 Conventions

Before introuding the research, I will clarify a few conventions and notations to be used throughout the paper:
• $\langle x, y \rangle$ represents a group generated by x and y.
• Composition of functions, in particular permutations, will always be shown as $f \circ g$. and the rightmost function is evaluated first.
• When two permutations are multiplied without use of an operator symbol, i.e. $\sigma\tau$, we evaluate from left to right, so computing σ then τ.

2 The square pillowcase

As shown below, the square pillowcase Z is the gluing by translation and 180 degree rotations of two squares, one labeled Q, the other the reflection of Q called $\bar{Q}$. It is defined as $Z := \mathbb{R}^2/\Gamma$ where $\Gamma := \{x \mapsto \pm x + (m, n) | m, n \in \mathbb{Z}\}$. The fundamental domain of Γ is given be the rectangle, $\{(0,0), (1,0), (0, \frac{1}{2}), (1, \frac{1}{2})\}$.

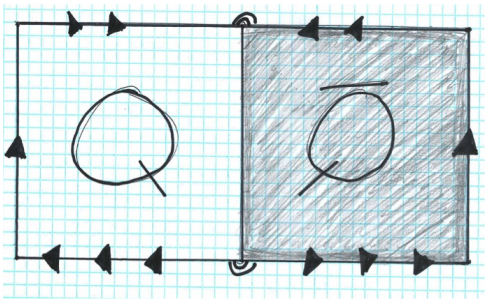

Figure 1: The square pillowcase

2.1 Geometry of the square pillowcase

The square pillowcase is homeomorphic to the sphere, i.e. there exists a one-to-one, onto, continuous map from Z to S^2 with continuous inverse.

Furthermore, geometry in the real plane induces a geometry on Z.

Lemma 1. *Any curve of rational slope on Z will close up, given that it does not intersect one of the corners.*

Proof. The group Γ acts on $\mathbb{R}^2$ and the group elements of Γ preserve slope. So for a rational slope curve in $\mathbb{R}^2$, there is a translation in Γ that sends it to the square pillowcase as a closed curve. □

Remark 4. It is interesting to note also that a rationally sloped curve with an orientation separates the corners as two on the left and two on the right.

One can also look at the group of affine symmetries on the square pillowcase. The transformations occurring in the real plane descend to a rich group of transformations of the square pillowcase.

Definition 10. The *affine group* on $\mathbb{R}^2$ is the set of automorphisms given by $Aff(\mathbb{R}^2) := \{f_{A,b}(x) = Ax + b | A \in GL_2(\mathbb{R}), b \in \mathbb{R}^2\}$.

Definition 11. For $x \in \mathbb{R}^2$, a *point* in the square pillowcase Z is $\Gamma.x$ the orbit of x under Γ.

Theorem 9. *The affine group of area preserving and orientation preserving automorphisms of the square pillowcase is $Aff^+(Z) := \{\bar{f}_{A,b}(\Gamma.x) = \Gamma.f_{A,b}(x) | A \in SL_2(\mathbb{Z}), b \in \frac{1}{2}\mathbb{Z}^2\}$.*

Proof. It is easy to check that this is a group. Closure and associativity follow from $Aff(\mathbb{R}^2)$ being a group. The identity element is $\bar{f}_{I,(0,0)}$. One can also find inverses: $(\bar{f}_{A,b})^{-1} = \bar{f}_{A^{-1},-A^{-1}b}$
Next we must show that $\bar{f}_{A,b}$ is well-defined, i.e the function does not depend on our choice of x:
$\bar{f}_{A,b}(\Gamma.x) = \Gamma.f_{A,b}(x) = \Gamma.(Ax + b)$
Now we send $x \mapsto x + (i, j)$ for $i, j \in \mathbb{Z}$.
$\bar{f}_{A,b}(\Gamma.(x+(i,j))) = \Gamma.f_{A,b}(x+(i,j)) = \Gamma.[A[x+(i,j)]+b] = \Gamma.[Ax+A(i,j)+b]$
Since $A(i, j) \in \mathbb{Z}^2$ and $\mathbb{Z}^2 \subset \Gamma$, $A(i, j) \in \Gamma$.
So $\bar{f}_{A,b}(\Gamma.(x + (i, j))) = \Gamma.(Ax + b)$ □

3 Covering spaces of the square pillowcase

Definition 12. A *square-tiled half translation surface*, STHTS, is a closed, connected surface obtained by gluing several squares together along their edges in pairs by translations and 180 degree rotations.

Definition 13. A *square-tiled half translation surface with a reflection structure*, STHTSwRS, is a STHTS that glues white and black squares such that each white edge is paired with exactly one black edge.

Definition 14. A *square-tiled half translation surface with a reflection structure and a labeling* is a STHTSwRS such that all white squares are labeled Q, and all black squares are labeled $\bar{Q}$, and the labels preserve the reflection structure.

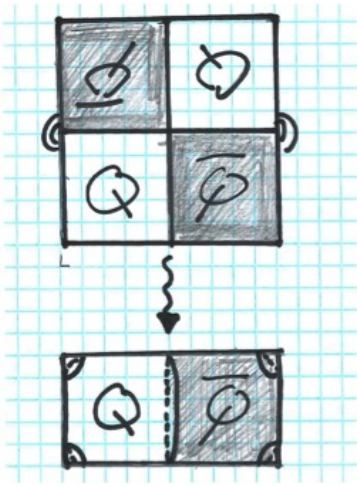

Figure 2: A *square-tiled half translation surface with a reflection structure and a labeling.* The top is an unfolding of the glued surface below.

There is an obvious map from a STHTSwRS+labeling to the square pillowcases that sends Qs in the cover to Q on Z and $\bar{Q}$s to $\bar{Q}$.

Definition 15. For X a STHTSwRS+labeling, a covering map of the square pillowcase is given by $f : X \longrightarrow Z$. We call this a *pillowcase cover*.

Remark 5. A STHTSwRS+labeling is equivalent to being a pillowcase cover.

4 Classification of pillowcase covers

In order to discuss the classification of pillowcase covers, we must first define the parameters by which pillowcase covers are classified.

Definition 16. The *degree* d of a pillowcase cover is half the total number of squares in the cover.

Definition 17. A *cone point* is a point whose angle is not equal to 2π.

Definition 18. If the angle of a cone point is $\frac{n\pi}{2}$, the *weight* of a cone point is n. We can also consider *weight* as the number of squares in the cover meeting at a cone point.

We also will use the *genus* of the surface to classify our pillowcase covers. The genus of a cover can be found using the *Euler Characteristic*:

$$\chi(X) = 2 - 2g = V - E + F$$

where g=genus, V=number of vertices, E=number of edges, F=number of faces.

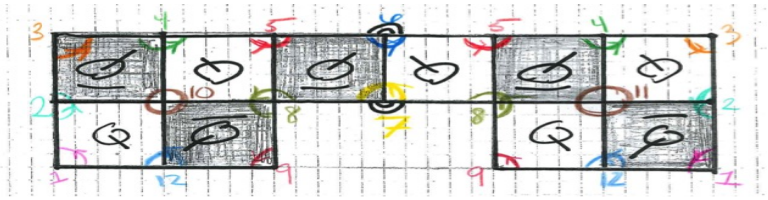

Figure 3: An example of a pillowcase cover X with an explanation of its classification below.

Example 2. There are 10 total squares so the *degree* d=5.
The colored numbers identify each vertex. From this we can determine the weight of each vertex. The vertices labeled 1, 3, 6, 7, and 9 have angle π. The vertices labeled 2, 4, 5, 10, 11, and 12 have angle 2π. And vertex 8 has angle 3π. Noting only vertices that are cone points, we can list the *weights* as such: (2, 2, 2, 2, 2, 6).
There are 12 vertices, 20 distinct edges (after gluing), and 10 faces. Thus the *Euler Characteristic* is $\chi(X) = V - E + F = 2$ and this implies the *genus* $g = 0$, so this cover is a sphere.

Definition 19. Two pillowcase covers $f : X \longrightarrow Z$ and $g : Y \longrightarrow Z$ are equivalent if there exists a preserving isomorphism $h : X \longrightarrow Y$. [4]

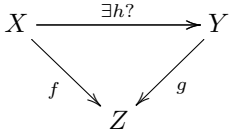

Proposition 10. *For two pillowcase covers $f : X \longrightarrow Z$ and $g : Y \longrightarrow Z$, if there exists such an equivalence $h : X \longrightarrow Y$, then h preserves the color of squares, labels, cone angles, and genus.*

5 Coding pillowcase covers

Definition 20. A *code* of a pillowcase cover of degree d is a bijection $\{squares\} \longrightarrow \{1, 2, 3, ..., 2d\}$ such that $\{white\} \mapsto \{odd\}$ and $\{black\} \mapsto \{even\}$.

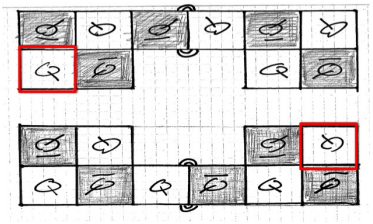

Figure 4: Example of two equivalent covers by mapping the red square in the top cover to the red square in the bottom cover.

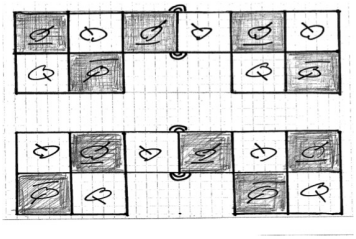

Figure 5: Example of two non-equivalent covers. There is no map between the two preserving color, labels, cone angles, and genus.

When representing a pillowcase cover by a diagram, we draw the numbers $\{1, 2, ..., 2d\}$ on squares such that the base of each number is the same as the base of Q or $\bar{Q}$, respectively. With this convention, given a code, we can reconstruct the labeling so that it is not necessary to draw both numbers and the Qs and $\bar{Q}$s.

To clarify some convention: The position of the label, whether Q, $\bar{Q}$, or a number, determines the top, bottom, right, and left edges of the squares. The top of the label matches the top of the square; the right side of the label matches the right edge of the square; and similarly for the left and bottom edges. When we say go *up* from a square, that means go through the top of that square. Going *down* means go through the bottom. Going *left* means go through the left edge of the square and similarly for going *right*.

Definition 21. The permutation $\sigma \in S_{2d}$ represents the horizontal permutation of a pillowcase cover. In cycle notation, σ always begins on an odd numbered square. Going right through the permutation is the same as going right from that square on the cover.

Definition 22. The permutation $\tau \in S_{2d}$ represents the vertical permutation of a pillowcase cover. In cycle notation, τ always begins on an odd numbered square. Beginning at an odd number, going right through the permutation is the same as going up from that square on the cover.

Remark 6. Due to the reflection structure of pillowcase covers, $\tau(odd)$ is going up from that square and $\tau(even)$ is going down from that square.

A code allows us to use a pair of permutations (σ, τ) to represent the cover.

Since implementing a code on a pillowcase cover requires a choice, we must define equivalence among codes so that any choice of code for the same pillowcase cover will be equivalent.

Two codes, (σ_1, τ_1) and (σ_2, τ_2) are equivalent if there exists $x \in S_{2d}$, $x(odd) = odd$ and $x(even) = even$, such that $\sigma_2 = x \circ \sigma_1 \circ x^{-1}$ and $\tau_2 = x \circ \tau_1 \circ x^{-1}$

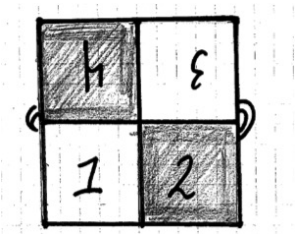

Figure 6: ($\sigma = (1234)$, $\tau = (14)(32)$)

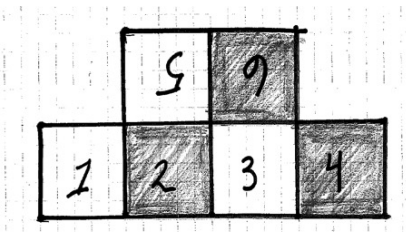

Figure 7: ($\sigma = (1234)(56)$, $\tau = (14)(3652)$)

Example 4. Let $\sigma_1 = (1234)$, $\tau_1 = (12)(34)$, and $\sigma_2 = (1432)$, $\tau_2 = (14)(32)$. Then the pillowcase covers given by (σ_1, τ_1) and (σ_2, τ_2) are equivalent by conjugation by $x = (13)$:
$\sigma_2 = x \circ \sigma_1 \circ x^{-1}$
$\tau 2 = x \circ \tau 1 \circ x^{-1}$

Theorem 11. *Two pillowcase covers, $f : X \longrightarrow Z$, $g : Y \longrightarrow Z$ are equivalent iff their codes are equivalent.*

6 Determining pillowcase covers algebraically

A code can be easily obtained when we have a surface X that is a pillowcase cover. Next we aim to build a convention that will allow us to understand and classify a pillowcase cover given only a pair of permutations (σ, τ).

Proposition 12. *A pair of permutation (σ, τ) is a pillowcase cover if:*
(i) $\sigma : odd \mapsto odd$ $\sigma : even \mapsto even$ $\tau : odd \mapsto odd$ $\tau : even \mapsto even$
(ii) The group generated by σ and τ acts transitively on $\{1, 2, ..., 2d\}$, i.e, for each $i, j \in 1, 2, ..., 2d$ there is a permutation $g \in \langle \sigma\tau \rangle$ such that $g.i = j$.

Remark 7. Given a pair (σ, τ) known to be a pillowcase cover, we inherently know the degree d of the cover since $\sigma, \tau \in S_{2d}$.

6.1 Monodromy action on codes

In order to continue to classify pillowcase covers by a code (σ, τ), we want to be able to determine the genus and weight of all cone angles. In order to do so we will define four functions that act on codes.

Definition 24. On the square pillowcase $\mathbb{R}^2/\Gamma$, let a, b, c, d be the points $(\frac{1}{2}, \frac{1}{2}), (0, \frac{1}{2}), (0, 0), (\frac{1}{2}, 0)$, respectively. Note, these are the four corners of the pillowcase.

Definition 25. Let be $\alpha, \beta, \gamma, \delta$ be respectively the loops based at the center of $(\frac{1}{4}, \frac{1}{4})$ of the face labeled Q on the square pillowcase. The loops encircle a, b, c, d on the left-hand side, respectively.

We get $\alpha, \beta, \gamma, \delta$ to be the following:
$\alpha = \sigma\tau^{-1}$
$\beta = \tau\sigma$
$\gamma = \sigma^{-1}\tau$
$\delta = \tau^{-1}\sigma^{-1}$
Note that here we are not using standard composition of function, instead we will compute from left to right.

The following pictures represent how we determined $\alpha, \beta, \gamma, \delta$:

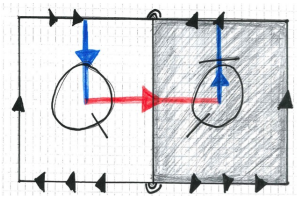

Figure 8: Loop around corner a at $(\frac{1}{2}, \frac{1}{2})$. Go right (red), then go up (blue).

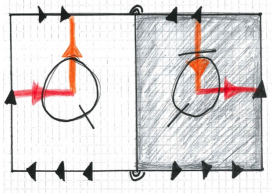

Figure 9: Loop around corner b at $(0, \frac{1}{2})$. Go up (orange), then go right (red).

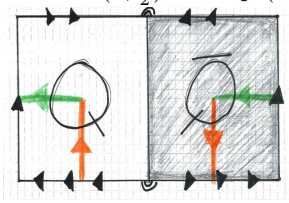

Figure 10: Loop around corner c at $(0, 0)$. Go left (green), then go down (orange).

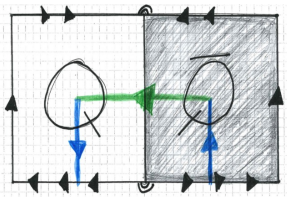

Figure 11: Loop around corner d at $(\frac{1}{2}, 0)$. Go down (blue), then go left (green).

Given these four functions, we can compute the monodromy of $\alpha, \beta, \gamma, \delta$ from the code of a pillowcase cover by only computing the restriction of $\alpha, \beta, \gamma, \delta$ to the odd numbers.

For a pillowcase cover $f : X \longrightarrow Z$ represented by a code (σ, τ), the monodromy of $\alpha, \beta, \gamma, \delta$ provides the following information:
• The total number of cycles in $\alpha, \beta, \gamma, \delta$ is the total number of vertices in the cover. Note: Cycles of length one also contribute to the total number of cycles.
• Each cycle length is the local degree of a vertex v, denoted $deg(f, v)$.
• The local degree of a vertex implies the weight of a cone point: $weight = 2deg(f, v)$.

At this point, for a pillowcase cover $f : X \longrightarrow Z$ given by a pair (σ, τ), we know the degree and weight of all cone points. We still wish to determine the genus of the cover. This can be done by computing the Euler Characteristic using the *Riemann-Hurwitz Formula*:

$$\chi(X) = deg(f)\chi(Z) - \sum_{v}(deg(f, v) - 1)$$

Note: $\chi(Z) = 2$ since Z our square pillowcase is homeomorphic to the sphere.

Example 5. We examine a pillowcase cover given by the pair of permutations $\sigma = (12345678)$ and $\tau = (12)(34)(56)(78)$:
•$\sigma, \tau \in S_8$ so the degree of the cover is $d = 4$.
• $\alpha = (1)(3)(5)(7)$, $\beta = (1357)$, $\gamma = (1753)$, and $\delta = (1)(3)(5)(7)$
• Using the cycle lengths of $\alpha, \beta, \gamma, \delta$ give us the local degree of vertices, so we can list the weights of each vertex: (2,2,2,2,2,2,2,8,8).
• Computing the Euler Characteristic: $\chi(X) = (4)(2) - [3 + 3] = 2$. Since $\chi(X) = 2 - 2g$ the genus of this cover is $g = 0$, so the surface is a sphere.

7 Action of the affine group on codes

Returning to the geometry of the square pillowcase and its group of affine symmetries, we are interested in observing how these symmetries affect codes by post composition.

Recall that the affine group of the square pillowcase is $Aff^+(Z) := \{\bar{f}_{A,b}(\Gamma.x) = \Gamma.(f_{A,b}(x)) | A \in SL_2(\mathbb{Z}), b \in \frac{1}{2}\mathbb{Z}^2\}$.
$Aff^+(Z)$ acts on equivalence classes of pillowcase covers by post-composition: $g.f := g \circ f$. So, $Aff^+(Z)$ acts on codes.

We are particularly interested in elements of the affine group that are in $PSL_2(\mathbb{Z}) = \langle \left(\begin{smallmatrix} 0 & -1 \\ 1 & 0 \end{smallmatrix}\right), \left(\begin{smallmatrix} 1 & 1 \\ 0 & 1 \end{smallmatrix}\right) \rangle$. These matrices that generate $PSL_2(\mathbb{Z})$ are respectively a counter clockwise 90 degree rotation and a sheer to the right.

Theorem 13. *Let* $A := \left(\begin{smallmatrix} 0 & -1 \\ 1 & 0 \end{smallmatrix}\right)$ *and* $B := \left(\begin{smallmatrix} 1 & 1 \\ 0 & 1 \end{smallmatrix}\right)$
For a given pillowcase cover (σ, τ) *we can compute:*
(i) $A.(\sigma, \tau) = (\sigma', \tau') = (\tau^{-1}, \sigma)$
(ii) $B.(\sigma, \tau) = (\sigma', \tau') = (\sigma,\ \sigma\tau^{-1}\sigma^{-1}$ *if odd and* τ *if even)*

Proof. We begin with sections of two arbitrary pillowcase covers with a code, as shown below. The letters i, j, k, l are elements in S_{2d}.

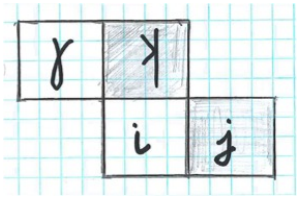

Figure 12: An arbitary cover, called X. We know $\sigma(i) = j$, $\sigma(k) = l$, and $\tau(i) = k$.

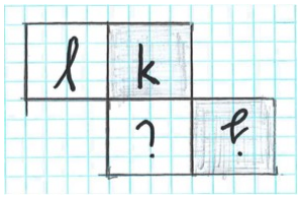

Figure 13: An arbitrary cover, called Y. We know $\sigma(l) = k$, $\sigma(j) = i$, and $\tau(k) = i$.

Since affine transformations are done post composition, we must apply the inverse of that transformation to the pillowcase cover in order to see how the code changes.
(i) Under the inverse of the rotation matrix A, the arbitrary cover X changes to:

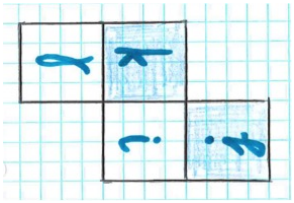

Figure 14: $\sigma'(k) = i$, $\tau'(i) = j$, and $\tau'(k) = l$.

and the abritrary cover Y changes to:

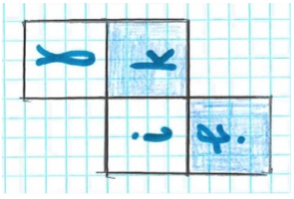

Figure 15: $\sigma'(i) = k$, $\tau'(j) = i$, and $\tau'(l) = k$.

From these new surfaces, we can see that $\sigma' = \tau^{-1}$ and $\tau' = \sigma$. Thus rotation

by 90 degrees affects codes in the following way: $A.(\sigma, \tau) = (\tau^{-1}, \sigma)$.
(ii) Under the inverse of the shear B, the arbitary cover X changes to:

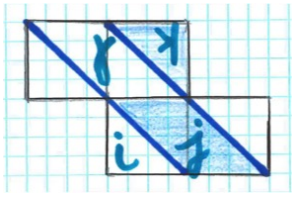

Figure 16: $sigma'(i) = j$, $\sigma'(k) = l$, and $\tau'(l) = j$.

and the arbitrary cover Y changes to:

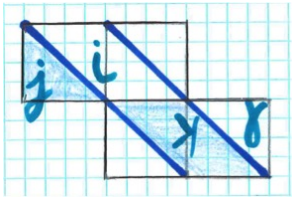

Figure 17: $sigma'(j) = i$, $\sigma'(l) = k$, and $\tau'(k) = i$.

From these new surfaces, it is easy to see that $\sigma' = sigma$. However, τ' does not act the same on white squares and black squares, or equivalently odd and even numbers. $\tau'(even) = \tau$ since $\tau'(k) = \tau(k) = i$. It is harder to define $\tau'(odd)$ in terms of σ, τ. Since $\tau'(l) = j$, the following picture uses the arbitrary cover X to show how $\langle \sigma, \tau \rangle$ send l to j:

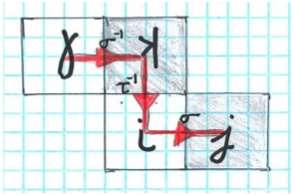

Figure 18: $\sigma \circ \tau^{-1} \circ \sigma^{-1}(l) = j$

Thus the right shear B affects codes in the following way:
$B.(\sigma, \tau) =$(σ, $\sigma \circ \tau^{-1} \circ \sigma^{-1}$ if odd or τ if even). □

7.1 Future work

We would like to continue looking into the effects of post-composition by these affine symmetries. In particular, future work will include computing stabilizers of this group as it acts on codes.

References

[1] Kathleen Moriarty, *Covering Spaces of the Punctured Torus* 2002

[2] Naomi Utgoff, *Affine Diffeomorphisms of Coverings of the Punctured Torus* 2002

[3] G. Schmithusen, *An Algorithm for Finding the Veech Group of an Origami*

[4] Allen Hatcher, *Algebraic Topology* 2001

Theorem[section] [theorem]Corollary [theorem]Lemma [theorem]Proposition [theorem]Definition

Developing an Algorithm for the Treatment of Elastic Networks

Andrew Henderson
Mentor: Professor Dylan Thurston
Indiana University, Bloomington

Abstract

In this project, elastic networks were defined as undirected graphs with weighted edges (rubber bands tied together are good examples of these networks). Stretching an elastic network in $\mathbb{R}^1$ can be thought of as being equivalent to an electrical network and can be examined using the techniques of computing the equivalent resistance across a network of resistors. The first problem this project approached was a Dirichlet problem involving an L-shaped graph.

Secondly, this project developed methods for embedding elastic networks inside "pipe graphs" which were defined as undirected graphs with edge weightings corresponding to lengths of pipes. In this case, the use of electrical methods breaks down as Kirchhoff's laws no longer apply. Thus, an algorithm was developed to numerically compute the energies of such embeddings. This algorithm was used to analyze the energies of graphs obtained by triangulating hexagons and it is able to accurately predict whether some hexagons can be embedded in others. In the future, we expect to generate graphs from tilings of other interesting surfaces.

1 Introduction

In this project, we were concerned with computing energies of elastic networks; we will begin with a definition of an Elastic Network.

Definition 26. Elastic Network an undirected, weighted graph.

An elastic network as defined can be thought of as a network of ideal springs. The weightings on the edges of the graphs correspond to the spring constants of the springs. These springs are ideal springs in that they have resting length 0 and they always obey Hooke's law (they are never deformed).

1.1 Resistor Networks

There is a simple correspondence between elastic networks and resistor networks. To see this, compare the form of Ohm's law to that of Hooke's Law.

Ohm's Law:

$$V = IR \quad \equiv \quad I = \frac{V}{R} \quad \equiv \quad I = CV$$

where I = current, V = Voltage, R = Resistance, and $C = \frac{1}{R}$ = Conductance.

Hooke's Law:

$$T = kX$$

where T = tension, k = spring constant, and X is displacement.

Here, we have
Tension $\rightarrow$ Current
Displacement $\rightarrow$ Voltage and
Spring Constant $\rightarrow$ Conductance

Then we have that the power dissipated through a resistor $P = IV = \frac{V}{R}V = V^2C$ which is analogous to the potential energy stored in a stretched spring $U = \frac{kX^2}{2}$

1.2 Finding Equilibrium

In this section, we are concerned with finding the optimal configuration of an elastic network when it is mapped to $\mathbb{R}^1$ (the interval $[0, 1]$).

Definition 27. Map (to interval) A map is a function which takes vertices of some elastic graph to a position

Definition 28. Position (Interval) A position in an interval is a real number paired with a Boolean

The Boolean describes whether the position is moveable. The definition of Position will be modified later, when the map destinations become more complicated. When mapping to the interval, each vertex is mapped to a position. These positions are analogous to the potentials at junctions in a resistor network. Some of the vertices are "pinned" to particular positions (represented by a Boolean False) which is analogous to applying a potential difference to some junctions in a resistor network. Our algorithm finds the optimal positions for these moveable vertices.

2 Developing an Algorithm

2.1 Binary Search

As a first attempt, we designed an algorithm using a binary search method. The algorithm follows

1. Given an elastic network and a map to the interval, the moveable vertices are identified.

2. Then, the signed sum of the tensions on each moveable vertex was computed and unbalanced vertices (sum $\neq 0$) were identified.

3. The most unbalanced vertex was balanced using a binary search algorithm.

4. This process was repeated until no unbalanced vertices remained.

This process was functional, but the vertex by vertex algorithm had intolerable runtimes with even relatively small numbers of vertices (n > 10). Thus, a different algorithm was developed.

2.2 Linear Equations

It is known that at equilibrium, the sum of tensions on any vertex must be zero (this is analogous to Kirchhoff's Current Law). Define T_{v_i,v_j} to be the tension on vertex v_i from v_j, let M be the set of moveable vertices in some graph, then:

$$\forall v_i \in M, \sum_{v_j \text{ adjacent to } v_i} T_{v_i,v_j} = 0 \tag{1}$$

When an elastic network is mapped to $\mathbb{R}^1$

$$T_{v_i,v_j} = \frac{p_j - p_i}{\alpha_{i,j}} \tag{2}$$

Where p_i is the position of v_i

Thus if there are n moveable vertices in M then we have a system of n linear equations of n variables which can be solved to find the equilibrium position of each vertex.

This algorithm generated the terms of these linear equations and put them into matrix form so that they could be solved using the Numeric Linear Algebra Package hmatrix for Haskell. When this system of linear equations was solved, the optimal position of each vertex was returned.

2.3 L-Shaped Graph

The first problem this algorithm was used to solve was a discrete Dirichlet problem which we referred to as an L-Shaped Graph

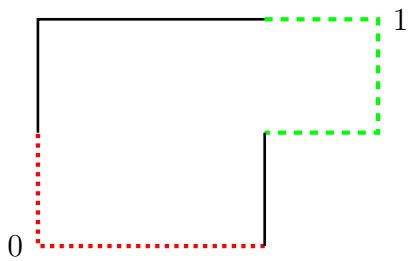

Above is a continuous Dirichlet problem. The region consists of the union of five congruent squares. The red (dotted) region is mapped to 0 and the green (dashed) region is mapped to 1 on the interval $[0, 1]$

First, we wanted to compute the effective resistance of graphs produced by tiling the shape with successively smaller squares and assigning unit resistance to the edges of each square.

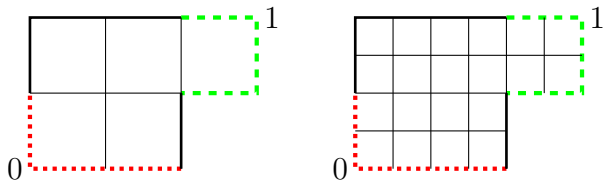

Above are the first two discretizations of the L-Shaped graph, n = 1 and n = 2. Each edge was assigned unit resistance and the linear algebra algorithm was used to compute the power dissipation through the network when the vertices on the dotted lines were set to voltage 0 and those on the dashed lines were set to voltage 1. This was then used to compute the effective resistance of the network. The effective resistance of the first 40 discretizations were computed. Unfortunately for higher values of n, the number of vertices grows too large to be effectively computed using dense matrices. Thus, we are of the precise limit of the sequence.

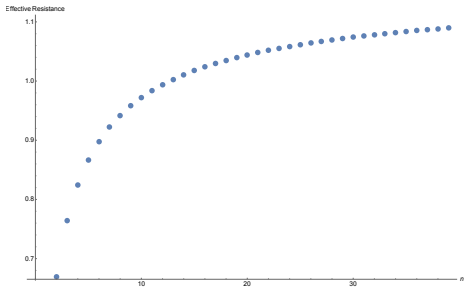

Second, we were interested in examining the behavior of the shape under factors of horizontal and vertical stretching.

Maxime Fortier Bourque showed that in the continuous case, the effective resistance of this figure remains bounded. His argument is summarized below.

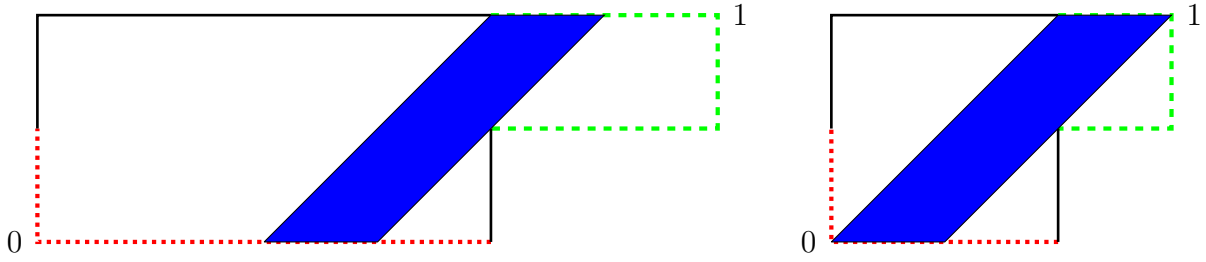

Under horizontal stretching, the blue region above will always be congruent to the same region in the original shape. Additionally, if we cut the white regions we can only have increased the effective resistance which implies that the blue region gives an upper bound on the effective resistance of the graph.

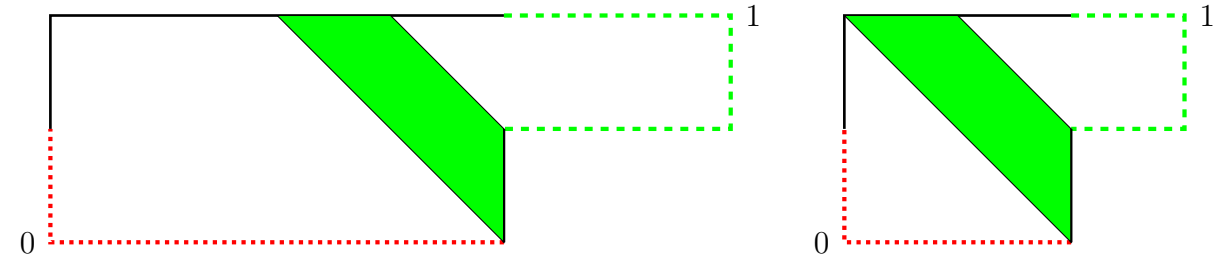

Again, the green shaded region is present regardless of horizontal stretching factors, thus if we short out the unshaded region we can only have decreased the resistance. Therefore the green region gives a lower bound on the effective resistance. Analogous arguments exist for vertical strech factors. Thus, we believe the effective resistance of the L-shaped region remains bounded under stretching.

In order to discretize the stretched versions of the L-Shaped region, we assigned modified resistances to the horizontal and vertical edges in the discretizations. When the shape was stretched horizontally by a factor of R, we assigned resistance R to the horizontal edges of the discretization and resistance $\frac{1}{R}$ to the vertical edges.

Unfortunately, the discretization breaks down unless $n >> R$ and our finite computational power limited our ability to compute varied values of R.

A suggestion for future work is to implement the linear solution function using sparse matrices which should improve runtime considerably and enable the effective computation of much finer discretizations.

3 Mapping to Pipe Graphs

The behavior of springs and resistors in $\mathbb{R}$ is well understood; however, motivations regarding conformal embedding of surfaces motivate examining elastic networks in other spaces. We were interested in describing the behavior of elastic networks embedded in graphs, prompting the following modified set of definitions

Definition 29. Pipe Graph A pipe graph is an undirected graph with weighted edges

The weightings on the edges of a pipe graph correspond to length

Definition 30. Map (to Pipes) A map is a function which takes elastic vertices to positions in pipes and elastic edges to paths through pipes.

Definition 31. Position (Pipe Graph) A position (in a pipe graph) is the location of an elastic vertex in a map. It includes a Boolean and either a target pipe (with a parameterized position on that pipe) or a target pipe vertex.

A good way to conceptualize these definitions is to consider the pipe graph as a plumbing system with the elastic network stretched through it in some way. The map contains all of the relevant information necessary to describe the positions of the elastic vertices in the pipes.

3.1 Modifying the Algorithm

The algorithm to find the optimal positions for the moveable vertices under some map was developed by extending the algorithm for the $\mathbb{R}^1$ case.

In this case, we still begin by solving a system of linear equations defined by the tension equations. The only modification necessary here is to keep track of the sign of the tension which corresponds to the orientation of the parameterization of the pipes (e.g. it is necessary to consider which end of the pipe each vertex is being pulled towards).

When an elastic vertex is mapped to a junction in the pipe system, there exists the possibility of a stable configuration which violates the tension equations. In this case, an elastic vertex will remain stationary unless the tension pulling it towards one pipe exceeds the sum of the tensions pulling in the other directions. We refer to this requirement as the generalized triangle inequality as it takes the same form as the triangle inequality when the number of pipes is equal to three.

With the exception of such pipe vertices, all other moveable vertices must satisfy the equilibrium of tensions, thus we can use linear algebra to solve for the positions of these vertices and then check the triangle inequality to see if any vertices violate the triangle inequality.

The solution to this system of equations, however, may yield degenerate solutions in which vertices are pulled past the ends of their target pipes. Thus, when this occurs, we "pull" the elastic vertex onto the pipe vertex.

By repeating this process until the triangle inequality is satisfied on all of the vertices and no degenerate positions remain, we find the optimal configuration of the elastic network, and thus its minimal energy.

3.2 Results

We chose to begin by mapping to the tripod. This graph consists of three edges joined at a single central vertex. This allows us to omit the information about paths because there is only one path connecting any two points on the tripod.

We began by computing energies of elastic graphs obtained by triangulating the regular hexagon and mapping them to the tripod.

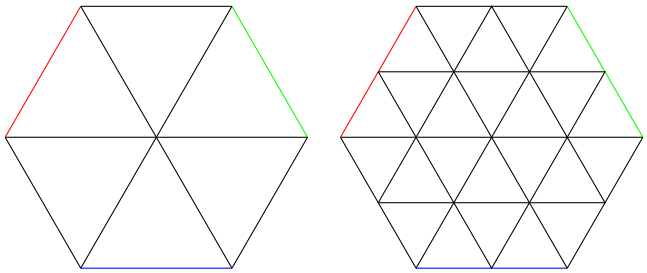

Above are the first two discretizations, n = 1 (left) and n = 2 (right). The vertices on each colored edge were sent to the ends of one of the tripods. $n-1$ refers to the number of vertices on each edge of the hexagon (e.g. there are 2 vertices on each mapped edge when n = 1).

We are interested in computing the energies of these meshes because we believe these energies are related to the existence of conformal embeddings. [1]

It is useful to compare the energies of multiple graphs over the space of possible tripod lengths. By fixing the sum of the lengths to 1, we get a two dimensional plot where x is the length of the first leg, y is the length of the second, and 1 - x - y is the length of the third.

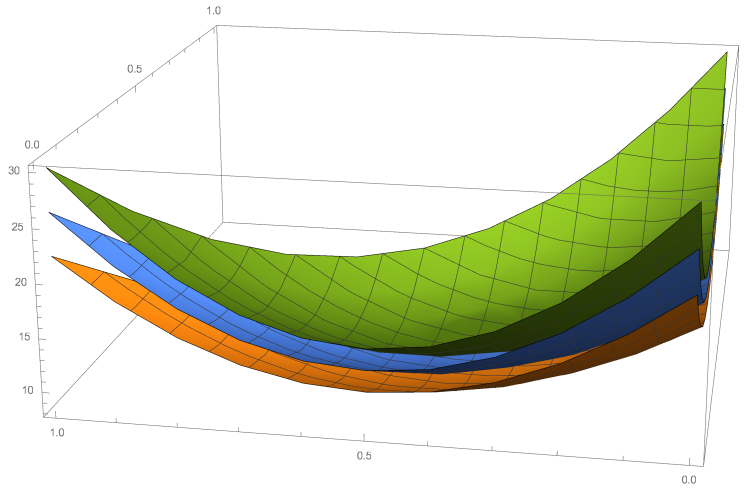

Above is a plot of the energies of three discretizations of the regular hexagon (from the bottom: n=5, n=6, and n= 7)

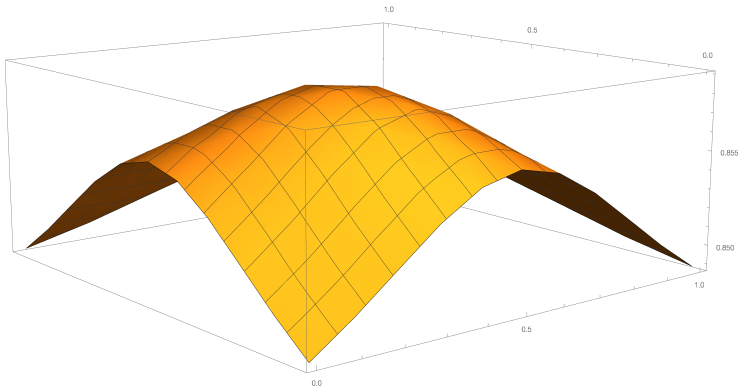

Above is a plot of the ratio of the energy of the n=5 case to that of the n = 6. The maximum value in the center of the plot indicates that the mesh converges fastest when the legs of the tripod are equal in length. Near the corners, the tripod approaches the interval and the difference between the iterations becomes more pronounced.

We then examined energies obtained by triangulating irregular hexagons with interior angles of 120°

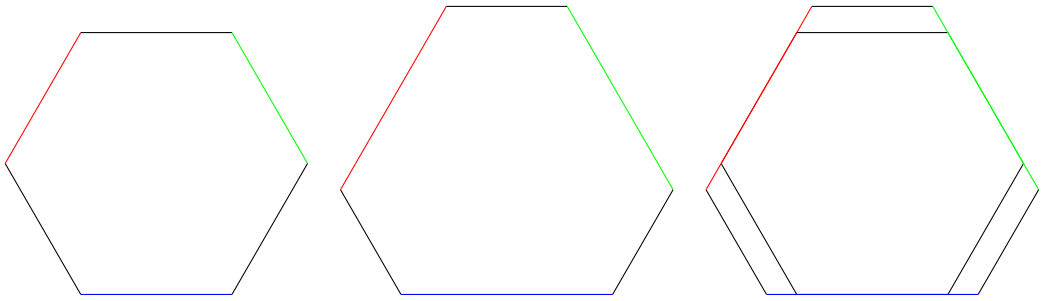

Here is one of the irregular hexagons we examined. Left is the regular hexagon. Middle is a hexagon on which three of the edges have been lengthened. Right shows an embedding of the regular hexagon inside the irregular one. We triangulated both of them using the same triangulation (n=10) and plotted their energies as we did before.

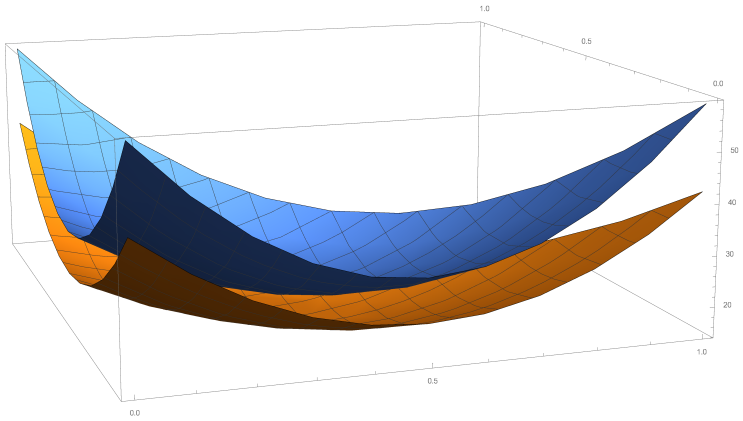

Above is a plot of the n=10 mesh on the regular hexagon (bottom) and the modified hexagon (top). We expect there to exist a conformal embedding of the regular hexagon in this modified hexagon. The experimental data agree with this expectation.

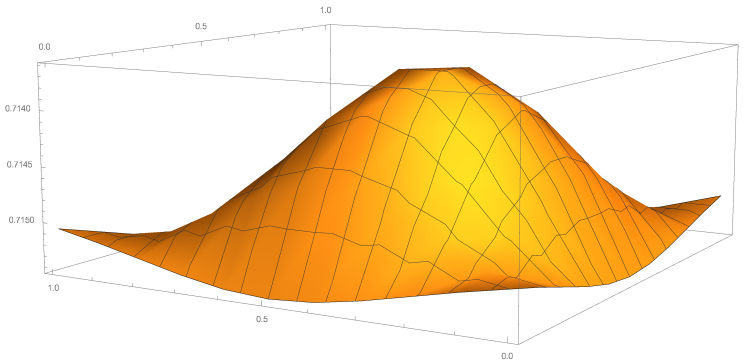

Above is a plot of the ratios between the n = 10 discretization and the modified hexagon. Again, we see that the energies are closest when the tripod legs are close to equal in length.

4 Conclusions

This program allows us to compute the energies of various graphs. We can evaluate graphs generated by triangulating the hexagon and the in the future we will examine graphs obtained by other surfaces in the hope of examining the existence of conformal embeddings.

References

[1] Jeremy Kahn, Kevin M. Pilgrim, Dylan P. Thurston, "Conformal Surface Embeddings and Extremal Length." 19 Jul 2015 http://arxiv.org/pdf/1507.05294v1.pdf, Accessed 30 July 2015

Theorem[section] [theorem]Proposition [theorem]Lemma [theorem]Corollary [theorem]Example [theorem]Remark
[theorem]Definition

Abstract

We investigate subgroups of the braid group conjugate to the wicket group as a way of obtaining stabilizer groups of various tangles. These groups, together with a generalization of the plat closure of a braid to closures by arbitrary tangles gives a new classification of $(2,1)$ triplane diagrams. In the future, it is possible that these techniques may be applied to open questions about higher bridge triplane diagrams.

Groups Conjugate to the Wicket Group and Classification of Triplane Diagrams

Sam Pilgrim

Introduction This paper presents a new proof of the classification of $(2,1)$ diagrams using a lower-tech, algebraic approach involving the braid group. We begin with an introduction to the terminology of classical knot theory, which will be used throughout this paper. We go on to introduce tangles, bridge splittings of knots, braids, and their closures. Using these tools, we develop a generalization of the plat closure of a braid. This generalization, together with an understanding of subgroups of the braid group that fix various tangles, allow us to classify $(2,1)$ triplane diagrams by studying how the braid group acts on them. The remarks at the end give a brief discussion of the application of this strategy to the 3 and $4-$bridge cases.

1 Knots and Links

Definition 32. A *knot* is an embedding of the circle, S^1, in S^3 (see figure 1).

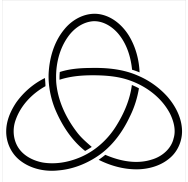

Figure 1: The trefoil – the simplest knot

If we want to make statements about equivalence or in-equivalence of 2 knots, we need to introduce an equivalence relation. We say that two knots are equivalent if there is an ambient isotopy between them. Intuitively, all this means is that one knot can be deformed into the other without breaking it anywhere or passing it through itself. This is exactly the type of equivalence we would wish to capture if we were thinking of knots tied out of string.

Next, we want to establish a notion of a knot being "untie-able" (and hence not a knot at all). If an embedding of S^1 is isotopic to a Euclidean circle, we call it unknotted, or simply an unknot.

A generalization of the definition of knot gives us the following:

Definition 33. A *link* consists of multiple embeddings of S^1 in S^3.

These copies of S^1 may be knotted or unknotted, and they may be linked together (see figure 2) or separable. We call n copies of the unknot, none of which are linked together an *unlink of n components*.

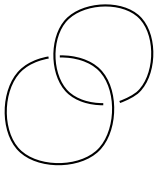

Figure 2: The Hopf Link – the simplest link

Although knots and links exist in 3−space, it is much more convenient if we can study them via diagrams in the plane such as our previous 2 figures. To that end, we give the following definition:

Definition 34. A *knot diagram* is the result of projecting a knot in (x, y, z) space onto the (x, y) plane. Any point where one arc of the knot passes over another (meaning that two points have the same x and y coordinates we call a crossing point. We call the arc containing the point with greater z coordinate the overstrand, and the arc containing the point with smaller z coordinate the understrand. At each crossing point, we add crossing information to our diagram by breaking the understrand.

We need to be sure that no information is lost during this projection. It is possible, for instance, that more than one strand passes directly under another, in which case more than 2 points in our original knot may be sent to the same point in the diagram. Furthermore, if the curve making up our knot is ever parallel to the z-axis, we end up sending infinitely-many points of our knot to a single point in the diagram.

The latter of these two problems may be resolved by applying an isotopy that rotates the knot slightly in 3−space. The former is fixed by perturbing (via isotopy) the understrands, changing the (x, y) coordinates slightly so that no

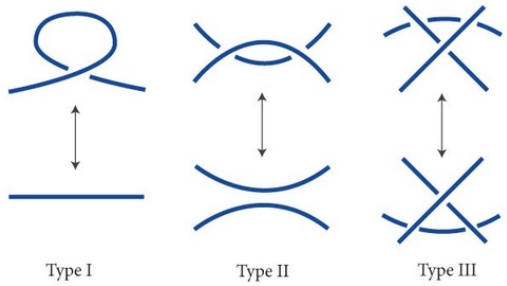

Figure 3: The Reidemeister moves

more than 2 points of the knot are sent to the same point in the plane. These arguments are explained in greater detail in [Liv93].

Now that we've established that a knot diagram can be constructed without any loss of information, we have that every knot (or link) has a unique diagram. We are therefore free to consider a knot and its diagram as interchangeable.

Finally, we would like to formalize a way to move between equivalent diagrams, thereby giving a geometric intuition to the concept of ambient isotopy that will allow us to make pictorial arguments about knots. The process of changing a diagram of a knot into another such that the two remain the same up to isotopy is captured by three types of geometric manipulations called *Reidemeister moves* (see figure 3). One can see that all three of these moves preserve the isotopy class of a knot (i.e. none of them involve breaking a strand or passing one strand through another).

If two diagrams represent equivalent knots, the two can be related by a series of Reidemeister moves. With this in hand, we may further say that equivalent diagrams represent equivalent knots. Our convenient way of studying knots as diagrams in the plane is therefore complete and ready to use.

2 Bridge Splittings of Knots

2.1 Bridge Position and Bridge Splittings

As a knot is a simple closed curve in S^3, it has local maxima and minima with respect to some height function, h. We therefore have the following definition.

Definition 35. Let K be an arbitrary knot (or link). If all minima of $h|_K$ occur below all maxima of $h|_K$, we say that K is in *bridge position* with respect to h (see figure 6).

We call the minimum possible number of such maxima the *bridge number* of K (the trefoil, for example is a $2-$bridge knot). Importantly, the number

of bridges (maxima) of a knot in bridge position is not necessarily the bridge number of the knot.

Definition 36. An *n−bridge tangle* is a set of n disjoint arcs embedded in a ball with their endpoints in the boundary of the ball. To make diagrams of tangles more comprehensible, we often flatten the part of the ball containing the endpoints so that the endpoints of the arcs appear to lie on a line, as in the example below.

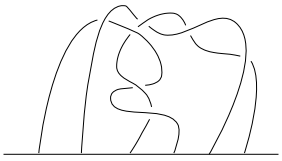

Figure 4: A 3−bridge tangle

As with knots, two tangles are equivalent if there is an ambient isotopy between them – though we require that such an isotopy fixes their endpoints.

A tangle consisting of n non-linking arcs is known as *the trivial tangle* (the 3−bridge trivial tangle is shown in figure 5). We also call any tangle trivial if its arcs can be simultaneously isotoped into the boundary of the ball (again without moving the endpoints). This is equivalent to these arcs, together with their images after such an isotopy, bounding disks, which we will call *bridge disks*. While trivial tangles are homeomorphic to *the* trivial tangle, they are not, in general, isotopic to it.

Figure 5: The 3−bridge trivial tangle

It should be clear that one can create a knot or link by taking a union of 2 n−bridge tangles that identifies the endpoints of one with the endpoints of another. Going the other direction, we now introduce a way that a knot may be split into a pair of tangles.

Definition 37. Let K be a knot or link in bridge position. Let $\Sigma \subset S^3$ be a 2−sphere that separates S^3 into two 3−balls. We call Σ the *bridge sphere*. The sets of disjoint arcs contained in each 3−ball are tangles, and if both tangles are trivial, we refer to Σ and the pair of tangles collectively as a *bridge splitting* of K (see figure 7).

Furthermore, there is always a way to split K such that the tangles obtained are trivial.

One can see from the example bellow (again involving the trefoil) that an $n-$bridge knot gives a pair of $n-$bridge tangles. We therefore call it an $n-$bridge splitting.

One can think of Σ as comprising all points in S^3 at some fixed height with respect to a height function. Thus, choosing different heights gives different spheres, and therefore different bridge splittings. When convenient, we may even assume that one tangle is the $n-$bridge trivial tangle, and that all the complexity of the knot lies in the other.

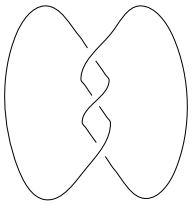

Figure 6: The trefoil in bridge position

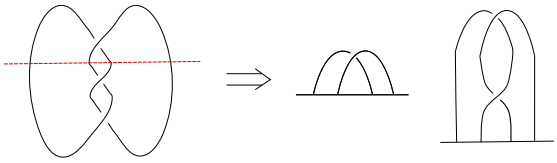

Figure 7: A bridge splitting of the trefoil and the resulting tangles – we represent the surface of Σ by the dashed red line

Definition 38. If a pair of arcs, one in each tangle of a bridge splitting, bound *bridge disks* that intersect each other exactly once in their boundary (see figure 8), we say that the bridge splitting is *stabilized* (refer to the following subsection and figures for more about stabilization).

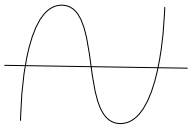

Figure 8: Bridge disks of this form are the result of stabilization, and can be removed through destabilization

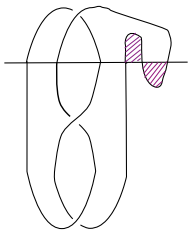

Figure 9: A stabilized bridge splitting of the trefoil

2.2 Equivalence of bridge splittings

Given 2 bridge splittings of the same knot, those splittings may be related by the following 3 types of moves:

1. Tangle isotopies – We may deform each of the tangles by an ambient isotopy (Reidemeister moves) that fixes the endpoints.

2. Bridge sphere braiding – We may perturb the bridge sphere so as to move the endpoints of each of the tangles around one another. This has the effect of braiding the loose ends of one tangle, and performing the opposite braiding on the ends of the other (braiding will be explained more fully in the section 4).

3. Stabilization/destabilization – We may deform a tangle to push it into the bridge sphere or pull it out, thereby adding or removing bridge disks of the type shown in figure 8.

2.3 Bridge splittings of the unknot

We conclude this section with a theorem about bridge splittings of the unknot.

Theorem 14. *[Ota82] Every bridge splitting of the unknot is stabilized.*

Though this theorem was previously known, we sketch a proof of it anyway.

Proof. Since the unknot bounds a disk, we begin by considering arbitrary intersections of the bridge sphere, Σ, with a disk, D. These come in two basic types. The first, represented by the blue arcs whose boundary points are contained in the boundary of D, denote intersections created by the disk "crashing through" the surface of the sphere (figure 10, left). The second type, represented by the purple circles, are created when part of the sphere "bubbles through" the surface of the disk (figure 10, right).

Next, we begin removing the purple circles one by one. We pick one circle with no others inside it. Since it bounds a smaller disk inside the surface of our original disk, we may perform surgery along it and discard the portion of the bridge sphere that doesn't intersect D anywhere else. Σ is still a sphere after surgery, and since the intersection we removed did not contain any part of the boundary of D, the new bridge sphere still gives the same bridge splitting. We

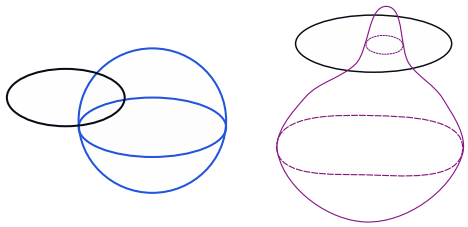

Figure 10: Two types of intersections of a sphere with a disk

repeat this process as many times as necessary until no more intersections of this type exist.

Through some additional deformation (see figure 11), we make our picture more familiar and obtain a stabilization of the unknot.

A consequence of this result (which can also be found in Otal), is that all $n-$bridge presentations of the unknot are equivalent through isotopies of tangles and bridge sphere braiding. The fact that stabilization is not necessary will be important later.

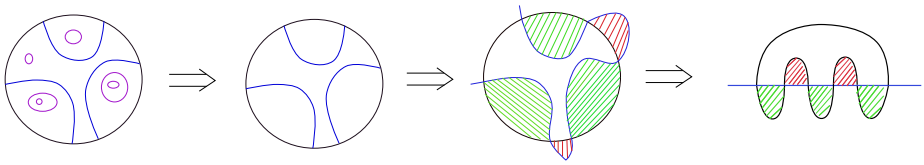

Figure 11: An arbitrary 3-bridge splitting of the unknot. Note that, no matter how we took this 3-bridge splitting, the result would be equivalent to the figure on the right by tangle isotopies and bridge sphere braiding.

□

3 Splittings in higher dimensions

Every embedding of S^1 in S^4 is unknotted, so if we want to discuss knots in four dimensions, we need to use knotted surfaces as opposed to knotted circles. Just like with classical knots in S^3, we can study these surfaces through a decomposition of the manifold in which they are embedded. In the case of surfaces in dimension 4, however, we split the $4-$sphere into three $4-$balls. This process leads us to the following definition.

Definition 39. A (b, c_1, c_2, c_3) *triplane diagram* is a triple of $b-$bridge tangles whose pairwise unions are unlinks of c_1, c_2, and c_3 components, respectively. If $c_1 = c_2 = c_3$, we refer to it simply as a (b, c) triplane diagram (see figures 12 and 13 for examples of (2,1) diagrams).

Triplane diagrams represent knotted surfaces in S^4. To see this, we can place the three tangles in figure 13 end to end (see figure 15) and imagine thickening the edges in their fourth coordinate. Moreover, since the knots formed by any two of the tangles in figure 15 are unknots (see figure 14), each of them bounds a disk, and so can be "capped off" with a disk to close the surface.

In this way, triplane diagrams can be viewed as a higher dimensional analog of bridge splittings of knots. For this reason, we may also refer to the triplane diagram of a knotted surface as a *bridge trisection*. This introduction to triplane diagrams is superficial, as the topological theory underlying them is complex, and outside the scope of this paper. Our goal here is to provide a relatively lower-tech approach to their classification.

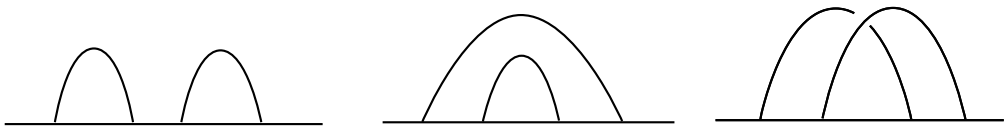

Figure 12: The triplane diagram of $\mathbb{R}P^2_+$

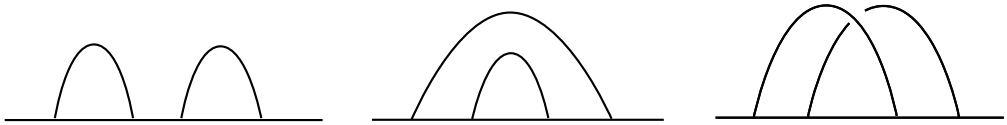

Figure 13: The triplane diagram of $\mathbb{R}P^2_-$

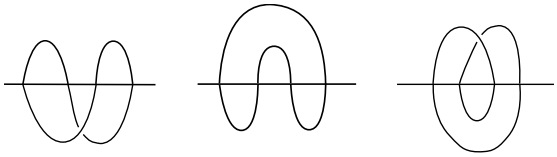

Figure 14: The pairwise unions of the tangles in the diagram of $\mathbb{R}P^2_-$. Notice that the tangles below are horizontal reflections of the tangles above.

Theorem 15. *All surfaces admitting a (2,1) bridge trisection are equivalent to one of two unknotted embeddings of* $\mathbb{R}P^2$.

Hence, all $(2,1)$ triplane diagrams are equivalent to one of the diagrams given above. Though this is already known, our main result will be a second proof in section 5 that uses a more direct, algebraic approach.

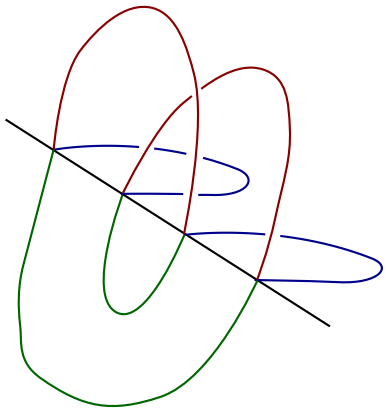

Figure 15: A triple of tangles giving rise to a surface

4 The Braid Group – B_n

4.1 Introduction

The braid group, B_n, is a group with an intuitive geometric interpretation – the braiding of n strings. Multiplication of braids is defined from left to right by appending them with the braid on the left at the top, and the identity is the trivial braid on n strands (n strands with no crossings).

Although infinite, B_n is finitely generated by elements s_i with $1 \leq i \leq n-1$, where s_i represents a positive half-twist between the i^{th} and $(i+1)^{st}$ strands.

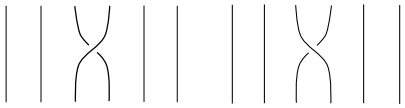

Figure 16: s_3 (left) and the inverse of s_3 (right), which we denote $\bar{s}_3$

The Braid Group also has 2 families of relations, namely

$$s_i s_j = s_j s_i \text{ when } |i-j| > 1, \text{ and}$$

$$s_i s_{i+1} s_i = s_{i+1} s_i s_{i+1}$$

Both of these relationships describe the ability to push twists along adjacent strands via isotopy (see figures 17 and 18), and thereby obtain an equivalent braid.

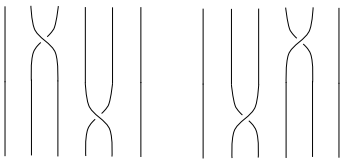

Figure 17: $s_i s_j = s_j s_i$ when $|i - j| > 1$

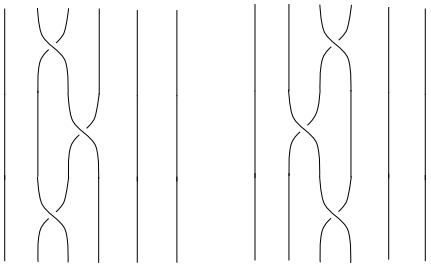

Figure 18: $s_i s_{i+1} s_i = s_{i+1} s_i s_{i+1}$

4.2 Actions of the braid group

B_{2n} acts on $n-$bridge tangles in the obvious way, that is, by braiding the loose ends at the bottom. If a is an $n-$bridge tangle and β is a $2n-$stranded braid acting on this tangle, we denote the resulting tangle by $a\beta$.

This action is also transitive, meaning that any $n-$bridge tangle can be turned into any other $n-$bridge tangle in this way. To see this, notice that any $n-$bridge tangle can be thought of as n non-linking arcs whose endpoints are braided in some way (see figure 19).

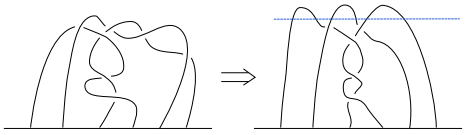

Figure 19: The $3-$bridge tangle shown earlier isotoped so that it appears as the $3-$bridge trivial tangle with some braid acting on it

Thus, the trivial tangle shown above the blue dashed line can be turned into any other tangle via braiding (in this example, the braid being applied in figure 17 is $s_2 s_4 \bar{s}_3^3$).

We now give notation for four tangles that will be used later (the tangles that appear in the triplane diagrams of $\mathbb{R}P^2_+$ and $\mathbb{R}P^2_-$):

We call the first tangle of each diagram (the tangle consisting of two non-

linking arcs) a_0, the second tangle (the one consisting of 2 nested, non-linking arcs) a_∞, the third tangle in the diagram of $\mathbb{R}P^2_+$, a_+, and the third tangle of the diagram of $\mathbb{R}P^2_-$, a_- (see figure 20).

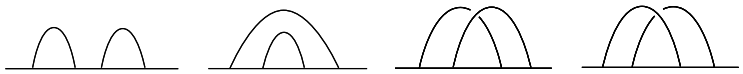

Figure 20: From left to right: a_0, a_∞, a_+, a_-

Transitivity of the action of B_{2n} tells us that all these tangles are related. In particular

$$a_\infty = a_0 s_2 s_3$$

$$a_+ = a_0 s_3$$

and

$$a_- = a_0 \bar{s}_3$$

These observations can be generalized to arbitrary tangles (again using transitivity), so we further have that, for any tangle b, $b = a_0\delta$ where δ is some braid [Taw08].

Since the process of taking the pairwise unions of tangles in a triplane diagram involves reflecting each tangle horizontally, we want to be able to talk about both a tangle and its image under such a reflection. Therefore, given a tangle a, let $\hat{a} = a$ and $\check{a}$ denote a reflected horizontally. If a and b are tangles, we may denote this aforementioned sort of union by $\hat{a}\check{b}$.

Notice that B_{2n} acts on $\hat{a}$ on the right and on $\check{a}$ on the left, so just as any tangle $\hat{a}$ can be written as $\hat{a}_0\delta$, any reflected tangle $\check{a}$ can be written as $\delta\check{a}_0$.

If a contains any crossings, those crossings will be reversed by a horizontal reflection which means that, if we apply a braid to $\hat{a}_0$ on the right and then reflect it, we will obtain the inverse of that braid acting on the left of $\check{a}_0$. For example, $\hat{a}_+ = \hat{a}_0 s_2$, so $\check{a}_+ = \bar{s}_2\check{a}_0$, which is the same as $\hat{a}_-$, albeit rotated by 180 degrees.

4.3 Stabilizers of tangles

As we have established how the braid group acts on tangles, we can now begin to discuss the *stabilizer groups* of tangles. The stabilizer group of an $n-$bridge tangle a, is the subgroup of B_{2n} with the property that, for β in this subgroup, $a\beta$ is isotopic to a. If this is the case, we say that β "fixes" a. We now introduce another group that will be critical to our discussion of stabilizers.

The wicket group, W_n, is a subgroup of B_{2n} preserving the configuration of n wickets. Thus W_n is the stabilizer group of the $n-$bridge trivial tangle (shown

below). In particular W_2 can be thought of as the stabilizer group of the tangle a_0.

W_n is generated by three families of elements: σ_i, ρ_i, and τ_j with $1 \leq i \leq n-1$ and $1 \leq j \leq n$ [BH13].

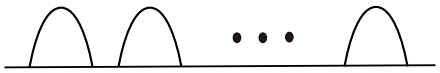

Intuitively, σ can be understood as representing passing one wicket over another, ρ as passing one wicket through another, and τ as putting a half-twist in one wicket.

W_n also has a number of relations, all of which come from B_{2n}:

$$[\tau_i, \tau_j] = 1 \text{ for } i \neq j$$
$$[\sigma_i, \tau_j] = 1 \text{ for } j \neq i, i+1 \text{ and } [\rho_i, \tau_j] = 1 \text{ for } j \neq i, i+1$$
$$\tau_i^\epsilon \sigma_i^\eta = \sigma_i^\eta \tau_{i+1}^\epsilon \text{ and } \tau_{i+1}^\epsilon \sigma_i^\eta = \sigma_i^\eta \tau_i^\epsilon \text{ for } \epsilon, \eta = \pm 1$$
$$\tau_i^\epsilon \rho_i = \rho_i \tau_{i+1}^\epsilon \text{ and } \tau_{i+1}^\epsilon \rho_i = \sigma^{-\epsilon} \bar{\rho} \sigma^\epsilon \tau_i^\epsilon.$$
$$\tau_{i+1}^\epsilon \bar{\rho}_i = \bar{\rho}_i \tau_i^\epsilon \text{ and } \tau_i^\epsilon \bar{\rho}_i = \sigma^{-\epsilon} \rho \sigma^\epsilon \tau_{i+1}^\epsilon$$

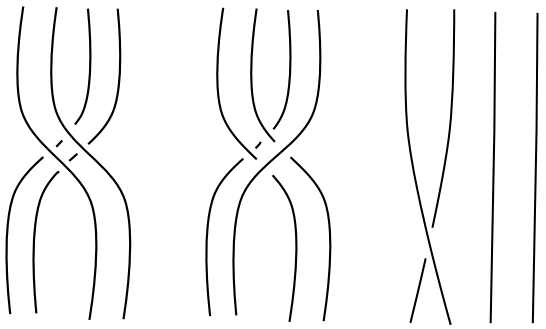

Figure 21: From left to right: σ, ρ, τ

4.4 Groups Conjugate to W_n

Now that we have a group of stabilizers for the first tangle of each of our triplane diagrams, we are interested in finding the stabilizers for the second tangle. Since tangles fixed by W_n as well as tangles of the form below appear not just in $(2,1)$ diagrams, but $(n,1)$ diagrams in general, we want to present this group in general before returning to the 2−bridge case.

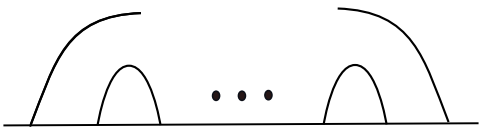

Recall that any $n-$bridge tangle b can be written as $a_0^n\delta$ where a_0^n is the $n-$bridge trivial tangle (the tangle fixed by W_n) and $\delta \in B_{2n}$. Then stabilizer groups of any tangle may be related to W_n by conjugacy.

In particular, we call the stabilizer group of the $n-$bridge tangle shown above W_n^∞. Let's call this tangle a_∞^n. Since $a_\infty^n = a_0^n s_2 s_3 \cdots s_{n-1}$, $W_n^\infty = \bar{s}_{n-1}\bar{s}_{n-2}\cdots\bar{s}_2 W_n s_2 s_3 \cdots s_{n-1}$. Essentially, a braid of this form sends a_∞^n to a_0^n, fixes a_0^n, then changes it back to a_∞^n.

Returning to the 2−bridge case, we have some additional examples of this which will be used later:

Let W_2^∞ be the stabilizer group of a_∞. Since $a_\infty = a_0 s_2 s_3$, $W_2^\infty = \bar{s}_3\bar{s}_2 W_2 s_2 s_3$.

Let W_2^+ be the stabilizer group of a_+. Since $a_+ = a_0 s_3$, $W_2^+ = \bar{s_3} W_2 s_3$.

Finally, let W_2^- be the stabilizer group of a_-. Since $a_- = a_0\bar{s}_3$, $W_2^- = s_3 W_2 \bar{s}_3$.

4.5 The intersection group − I_n

Now that we have the stabilizer groups of a_0 and a_∞, we can find the stabilizer group of all $(2,1)$ triplane diagrams (see the beginning of section 5 for an explanation of braid group action on triplane diagrams).

Definition 40. Let $I_n = W_n \cap W_n^\infty$

$$I_2 = \langle \tau_1\bar{\tau}_2, \rho, \sigma\tau_1^2 \rangle$$

We claim that this set of elements in I_2 is generating, which we will prove using the following lemmas. For now, it can be verified that these elements of W_2 are in I_2 by showing pictorially that they preserve a_∞.

The lemmas that follow present 2 useful facts about I_2, both of which will be used in our proof in section 5.

Definition 41. We call $w \in W_n$ *twist* if $w\tau_j^{k_j} \in I_n$ for $1 \le j \le n$ and $k \in \mathbb{Z}$.

Lemma 2. *$w \in W_n$ is twist if and only if $w = i\tau_j^{k_j}$ where $i \in I_n$.*

Proof. $\Rightarrow$: If $w\tau_j^{k_j} \in I_n$, then $w = w\tau_j^{k_j}\tau_j^{-k_j} = i\tau_j^{-k_j}$.

$\Leftarrow$: If $w = i\tau_j^{k_j}$, then $w\tau_j^{-k_j} \in I_n$ and w is therefore twist. □

Lemma 3. *All $w \in W_2$ are twist.*

Proof. Let $w \in W_2$. Using the wicket group relations to push any τ's to the right hand side, we may assume $w = w'\tau_1^k\tau_2^l$ where w' is a word in σ and ρ. We begin by looking at the letters of w' from left to right. Since $\rho \in I_2$, we can assume the first letter is σ. Now, $\sigma\tau_1^2 \in I_2$ and $\sigma\tau_2^2 \in I_2$, so we can insert either the canceling pair $\tau_1^2\bar{\tau}_1^2$ or $\tau_2^2\bar{\tau}_2^2$. However, when we try to push our extra τ's to the right (and in particular, past the first ρ appearing in w'), we may add additional σ's in front of the first ρ, which means our process will never end. We therefore want to choose our canceling pairs so that, by the time each τ is

immediately to the left of the first ρ, its index is one (or two if it's $\bar{\rho}$) instead of ρ. We can then move all of these τ's to the end of w. One can see that it really doesn't matter how many σ's are between each ρ, as long as we can "get past" the first ρ. Even if that involves adding 100 more σ's in front of the next one, we know our process will eventually terminate because eventually there will be no ρ's left.

More formally, let $w' = \sigma^k \rho^\epsilon \cdots$ where $\epsilon = \pm 1$.

If k is even and $\epsilon = 1$, or if k is odd and $\epsilon = -1$, we write $w' = \sigma\tau_2^2\tau_2^{-2}\sigma^{k-1}\rho^\epsilon \cdots$.

If k is odd and $\epsilon = 1$ or if k is even and $\epsilon = -1$, we write $w' = \sigma\tau_1^2\tau_1^{-2}\sigma^{k-1}\rho^\epsilon \cdots$.

Doing this for every σ, we obtain $w' = (\prod_{k=1}^{k} \sigma\tau_i^2)\rho^\epsilon \tau_j^{-2k} \cdots$ where $i = 1$ when k is even and $\epsilon = -1$ or k is odd and $\epsilon = 1$ and $i = 2$ when k is even and $\epsilon = 1$ or k is odd and $\epsilon = -1$ and $j = 1$ when $\epsilon = -1$ and $j = 2$ when $\epsilon = 1$.

Since $(\prod_{k=1}^{k} \sigma\tau_i^2)\rho^\epsilon \in I_2$, we now have $w' = i\tau_j^{-2k} \cdots$. We push τ_j^{-2k} to the end of w', possibly adding additional σ's, but not ρ's. We can then look further along the letters of w' until we see the next ρ, at which point this process can be repeated. □

Theorem 16. *I_2 is generated by $\tau_1\bar{\tau}_2$, ρ, and $\sigma\tau_1^2$.*

Proof. Let $w \in W_2$. By our lemma 4.4, we have that $w = i\tau_1^k\tau_2^l$. Since $\tau_1\bar{\tau}_2 \in I_2$, we have $w = i'\tau_1^{k+l}$.

It remains to be shown that $\tau^{k+l} \notin I_2$ unless $k + l = 0$. We do this by showing that $\hat{a}_\infty\tau_1^{k+l} \neq \hat{a}_\infty$ unless $k + l = 0$.

If $\hat{a}_\infty\tau_1^{k+l} = \hat{a}_\infty$, then $\hat{a}_\infty\tau_1^{k+l}\check{a}_\infty$ is an unlink of two components (see figure 22). We first note that if $k + l$ is odd, $\hat{a}_\infty\tau_1^{k+l}\check{a}_\infty$ is a knot, so we may assume $k + l$ is even. Next, we see that the linking number of $\hat{a}_\infty\tau_1^{k+l}\check{a}_\infty$ is precisely $-(l+k)/2$ (our conventions regarding τ_i and s_i are some confusing, as $\tau_i = \bar{s}_{2i-1}$) . Since the unlink of 2 components has linking number 0, $\hat{a}_\infty\tau_1^{k+l}\check{a}_\infty$ is an unlink of two components exactly when $l + k = 0$. □

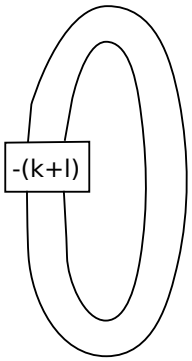

Figure 22: $\hat{a}_\infty\tau_1^{k+l}\check{a}_\infty$

Lemma 4. *$I_2 \subset W_2^+$ and $I_2 \subset W_2^-$.*

Proof. To see this, we simply note that the generators of I_2 all fix a_+ and a_-. □

We now take a brief detour to obtain some classification results from our generating set for I_2.

4.6 Classification of 2−bridge tangles with closures to the unknot

The generators of I_2 give a complete list of 2−bridge tangles whose unions with both $\check{a}_0$ and $\check{a}_\infty$ are the unknot (see figure 23).

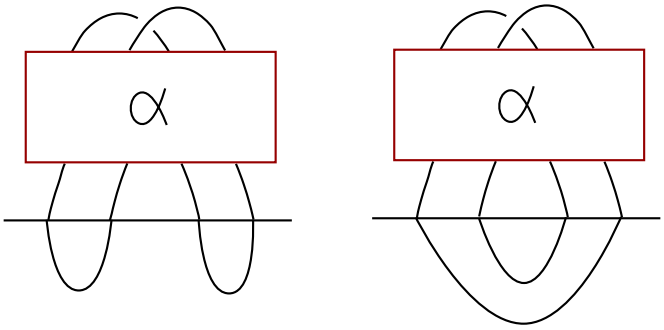

Figure 23: If $\alpha \in I_2$, both of these knots are the unknot

Furthermore, given a braid α' whose plat and shifted plat closures (see figure 24) are both the unknot, one can change this closed braid into one of the closed tangles in figure 23. Thus, we also have a list of all braids whose plat closure and shifted plat closure are the unknot.

4.7 Closures of braids

A braid α can be closed by connecting the loose ends at the top and bottom in various ways to give a knot or a link. In particular, the closure obtained by connecting the adjacent strands at the top and bottom is known as the *plat closure* of α. With the notation introduced in subsection 4.2, we may write the plat closure of a 4−stranded braid α as $\hat{a}_0 \alpha \check{a}_0$.

Theorem 17. *[Taw08] Given a knot or link L, there exists a (non-unique) $2n-$stranded braid α such that the plat closure of α is L.*

This follows from the fact that any knot or link can be put in bridge position.

We can now use our new notation to generalize this theorem to closures by arbitrary tangles, which we do in the following corollary.

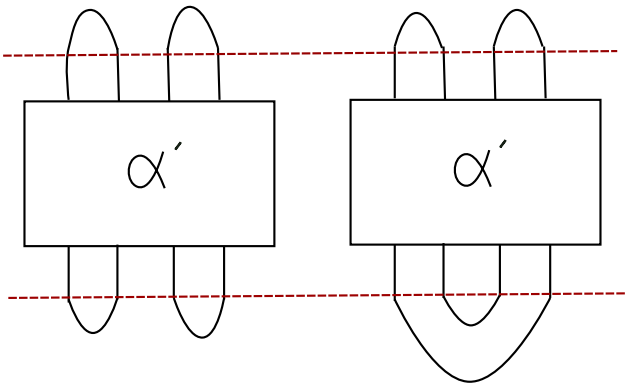

Figure 24: Plat closure and shifted plat closure of α'

Corollary 18. *Given a knot or link L, there exists a (non-unique) $2n-$stranded braid α such that $\hat{b}_1\alpha\check{b}_2$ is L and b_1 and b_2 are two $n-$bridge tangles.*

Proof. We have that $L = \hat{a}_0\alpha\check{a}_0$. By inserting canceling pairs of braids and using transitivity of braid group action on tangles, we obtain $L = \hat{a}_0\delta\bar{\delta}\alpha\bar{\delta}'\delta'\check{a}_0$ such that $\hat{a}_0\delta = \hat{b}$ and $\delta'\check{a}_0 = \check{b}_2$. Thus we have $L = \hat{b}_1\alpha'\check{b}_2$ and the proof is complete. □

As a further consequence of Theorem 2.4, we can now present the following lemma about braid closures to the unknot.

Lemma 5. *If t_0 and t_1 are two $n-$bridge tangles such that $\hat{t}_0\check{t}_1$ is the unknot and α is a $2n-$stranded braid such that $\hat{t}_0\alpha\check{t}_1$ is the unknot, then $\alpha = \beta_0\beta_1$ where β_0 and β_1 are stabilizers of t_0 and t_1 respectively.*

Proof. We suppose $\hat{t}_0\alpha\check{t}_1$ is the unknot and take an arbitrary bridge splitting. By Theorem 2.4, our bridge splitting is equivalent to $\hat{t}_0\check{t}_1$ via tangle isotopies and bridge sphere braiding. Thus, there exists a braid $\gamma \in B_{2n}$ such that $\hat{t}_0\alpha\gamma$ is isotopic to $\hat{t}_0$ and $\bar{\gamma}\check{t}_1$ is isotopic to $\check{t}_1$.

Then $\bar{\gamma}$ is a stabilizer of $\check{t}_1$ (and hence γ is a stabilizer of $\hat{t}_1$ via a horizontal reflection) and $\alpha\gamma$ is a stabilizer of $\hat{t}_0$. This implies that $\gamma = \beta_1$ and $\alpha\gamma = \beta_0$ and therefore that $\alpha = \beta_0\bar{\beta}_1$, which is what we wanted to show. □

We now have all the tools we need to present our main result.

5 Classification of $(2,1)$ triplane diagrams

Theorem 19. *All surfaces that give a (2,1) triplane diagram are unknotted embeddings of either $\mathbb{R}P^2_+$ or $\mathbb{R}P^2_-$.*

Proof. Let P be the triplane diagram of $\mathbb{R}P^2_+$. Since B_4 acts transitively on $2-$*bridge* tangles, it also acts transitively on $2-$bridge triplane diagrams.

Let P_α be the triplane diagram resulting from the action of $\alpha \in B_4$ on P. As with bridge splittings of classical knots, we may assume that all the complexity is contained in the final tangle (see figure 26). Our proof amounts to showing that if P_α is another (2,1) diagram, then P_α is the diagram of either $\mathbb{R}P^2_+$ or $\mathbb{R}P^2_-$

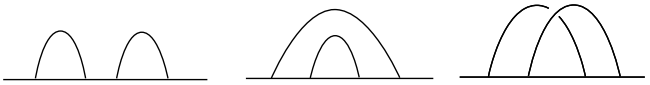

Figure 25: P

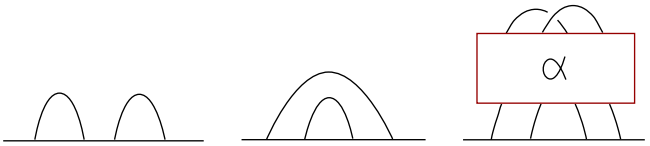

Figure 26: P_α

Let $\beta^0 \in W_2$, $\beta^\infty \in W_2^\infty$, and $\beta^+ \in W_2^+$

Let α be a braid such that P_α is another $(2,1)$ diagram. Then the pairwise unions of the tangles in P_α are unknots.

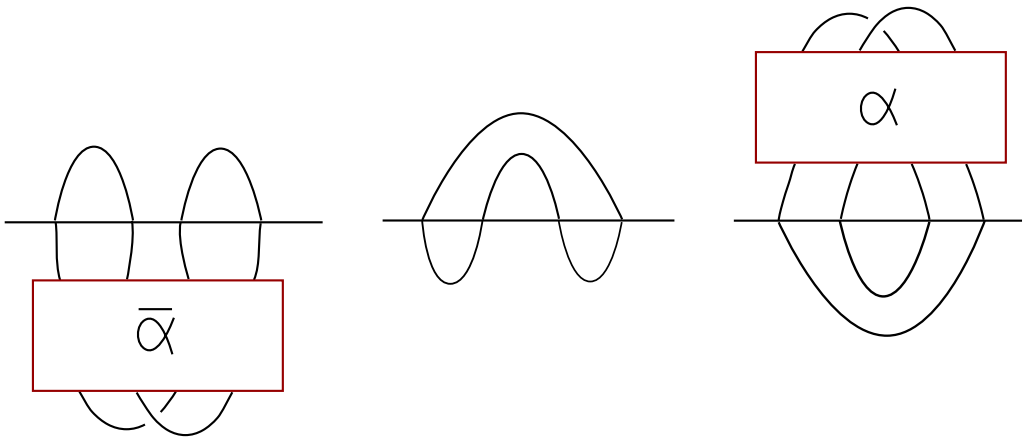

Figure 27: The pairwise unions of the tangles in P_α.

Since $\hat{a}_+ \alpha \check{a}_\infty$ is the unknot, lemma 4.9 implies that $\alpha = \beta_1^+ \beta^\infty$

Since $\hat{a}_0\bar{\alpha}\check{a}_+$ is the unknot, so is it's reflection $\hat{a}_+\alpha\check{a}_0$, so we further have that $\alpha = \beta_2^+\beta^0 = \beta_1^+\beta_2^\infty$.

$$\begin{array}{c}\text{Since } \beta_2^+\beta^0 = \beta_1^+\beta^\infty \\ \bar{\beta}_1^+\beta_2^+ = \beta^\infty\bar{\beta}^0\end{array}$$

So $\hat{a}_\infty\bar{\beta}_1^+\beta_2^+\check{a}_0$ is the unknot.
Since $\bar{\beta}_1^+\beta_2^+ \in W_2^+$, $\bar{\beta}_1^+\beta_2^+ = \bar{s}_2 w^0 s_2$ for $w^0 \in W_2$
By Lemma 4.4, we can write $\bar{\beta}_1^+\beta_2^+ = \bar{s}_2 i\tau_1^k s_2$
Thus, $\hat{a}_\infty\bar{s}_2 i\tau_1^k s_2\check{a}_0$ is the unknot.

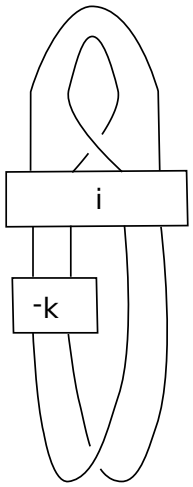

Figure 28: $\hat{a}_\infty\bar{s}_2 i\tau_1^k s_2\check{a}_0$

If k is odd, $\hat{a}_\infty\bar{s}_2 i\tau_1^k s_2\check{a}_0$ is a link of > 1 components, so we know k must be even.

Since $\bar{s}_2 i$ fixes $\hat{a}_\infty$, we see by an isotopy that the resulting knot is a torus knot with $-k-1$ crossings (see figure 29). Since the resulting diagram will be alternating (possibly after eliminating the first crossing at the top), we know that it is a minimal-crossing diagram for the resulting knot. Therefore, it is the unknot exactly when the number of crossings is < 3. This happens when $k = 0$ or $k = -2$. The argument then breaks down into handling each of these cases.

Case 1: $k = 0$ If $k = 0$, $\bar{\beta}_1^+\beta_2^+ = \bar{s}_2 i s_2$, which fixes $\hat{a}_\infty$. So $\bar{\beta}_1^+\beta_2^+ \in W_2^\infty$.

Therefore, $\bar{\beta}^\infty\bar{\beta}_1^+\beta_2^+ \in W_2^\infty$. But then $\bar{\beta}^0 \in W_2^\infty$, and is thus in I_2.

Since $\beta^0 \in I_2$ and $\alpha = \beta_2^+\beta^0$, $\alpha \in W_2^+$ by lemma 4.6, and we may conclude that $P_\alpha = P$.

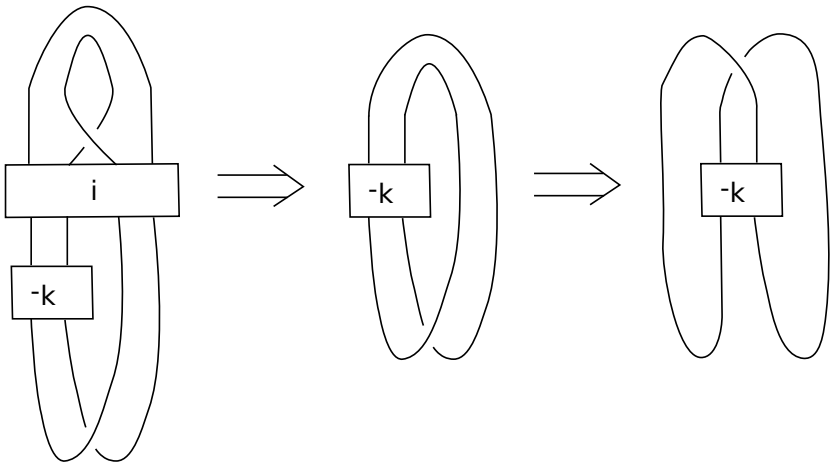

Figure 29: Simplifying the resulting knot

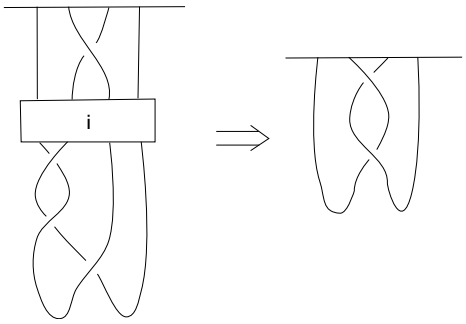

Figure 30: Simplifying $\bar{s}_2 i \tau_1^{-2} s_2 \check{a}_0$

Case 2: $k = -2$ If $k = -2$, we can see geometrically (see figure 30 and recall that $I_2 \subset W_2^-$) that $\bar{s}_2 i \tau_1^k s_2 \check{a}_0 = \bar{s}_2^2 \check{a}_0$, so $\bar{\beta}_1^+ \beta_2^+ = \bar{s}_2^2 w^0$ for some $w^0 \in W_2$.

So

$$\bar{s}_2^2 = \beta^\infty (\bar{\beta}^0 \bar{w}^0),$$

and

$$1 = (s_2^2 \beta^\infty)(\bar{\beta}^0 \bar{w}^0).$$

Since $s_2^2 \in W_2^\infty$, $\bar{\beta}^0 \bar{w}^0 \in W_2$, and $1 \in W_2$, we have that $s_2^2 \beta^\infty \in W_2$ and thus that $s_2^2 \beta^\infty \in I_2$.

So

$$s_2^2 \beta^\infty = j \text{ for some } j \in I_2$$

.

Then

$$\beta^{\infty} = \bar{s}_2^2 j$$

and we have

$$\alpha = \beta_1^+ \bar{s}_2^2 j$$

Since $\hat{a}_+ s_2^2 = \hat{a}_-$, j fixes $\hat{a}_-$, and P is the triplane diagram of $\mathbb{R}P^2_+$, we conclude that P_α is the triplane diagram of $\mathbb{R}P^2_-$

Thus, we have shown that, if P_α is a (2,1) diagram, then P_α is the diagram associated to an unknotted embedding of either $\mathbb{R}P^2_+$ or $\mathbb{R}P^2_-$. It follows that all (2,1) triplane diagrams represent unknotted surfaces. □

6 Remarks

It has been previously established that all (b, n) triplane diagrams with $b \leq 3$ represent unknotted surfaces, and that all $(b, 1)$ triplane diagrams represent topologically unknotted surfaces. A number of difficulties arise when applying these algebraic techniques to the classification of $(3, 1)$ diagrams. In particular, most elements of W_3 are not twist. Consequently, we do not have a convenient normal form for writing elements of W_3 as we did in the $2-$bridge case. However, a successful application of this style of argument to higher-bridge triplane diagrams may give an explanation as to why not all $(4, 1)$ diagrams represent smoothly unknotted surfaces.

References

[BH13] Tara E. Brendle and Allen Hatcher, *Configuration spaces of rings and wickets*, Comment. Math. Helv. **88** (2013), no. 1, 131–162.

[Liv93] Charles Livingston, *Knot theory*, The Mathematical Association of America, 1529 Eighteenth Street, NW Washington, DC 20036, 1993.

[Ota82] Jean-Pierre Otal, *Presentations en ponts du noeud trivial*, C. R. Math. Acad. Sci. Paris **294** (1982), no. 16, 553–556.

[Taw08] Stephen James Tawn, *Plat closure of braids*, Ph.D. thesis, University of Warwick, 2008.

Theorem[section] [theorem]Lemma [theorem]Example [theorem]Problem Definition

Degree 2 covers of the regular octagon and double pentagon translation surfaces

Zachary Wampler

1 Introduction

Many properties of translation surfaces have been discovered by investigating their $SL(2,\mathbb{R})$-orbit closures. The translation surfaces of a genus g which have closed $SL(2,\mathbb{R})$ orbit, called Veech surfaces, have especially nice properties. In this paper, we compute the $SL(2,\mathbb{R})$-orbits of degree 2 covers of two Veech surfaces: the regular octagon and double pentagon translation surfaces, X_8 and X_5.

2 Translation surfaces

Here, we define a few types of surfaces which will help us analyze X_8 and X_5.[1]

Definition 42. A *Euclidean cone* is a space obtained by cyclically gluing together a finite number of sectors. The *cone angle* is the sum of the angles of the sectors in the gluing construction. The *cone point* is the image of the origin under the gluing.

For example, if we glue together three quadrants of $\mathbb{R}^2$, each of these being a sector of angle $\pi/2$, we get a Euclidean cone with cone angle $3\pi/2$.

Definition 43. A *Euclidean cone surface* is a compact, oriented surface X such that

(i) Every point $x \in X$ has a neighborhood which is isometric to a neighborhood of the cone point in a Euclidean cone

(ii) All but finitely many points have neighborhoods which are isometric to the Euclidean plane

Definition 44. A translation surface is a collection of polygons with pairs of parallel edges identified in such a way that the identifications are restrictions of translations, every edge is identified with exactly one other edge, and when two edges are identified, their normal vectors point in opposite directions.

[1] The first two definitions here are taken from [1].

It follows that a translation surface is a Euclidean cone surface with a finite number of cone points, all of whose cone angles are integer multiples of 2π.

2.1 The regular octagon surface

Let X_8 denote the translation surface obtained by gluing together opposite sides of a regular octagon.

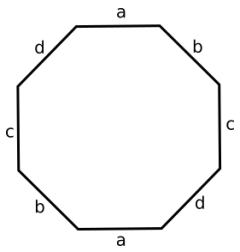

By following the edge identifications, we see that the resulting surface has a single cone point with cone angle 6π. Using the formula $2 - 2g = V - E + F$, where g is the genus of the surface, V the number of vertices, E the number of edges, and F the number of faces, we can determine the genus of X_8:

$$2 - 2g = 1 - 4 + 1$$
$$\Leftrightarrow g = 2$$

2.2 The double pentagon

For odd n, there is a family of "double n-gon" translation surfaces, each of these consisting of a pair of regular n-gons with a single edge of the first glued to a single edge of the second. The double 5-gon, X_5, like the octogaon, is a genus 2 translation surface with a single cone point with cone angle 6π. To determine what distinguises X_5 from X_8, we will take a look at their images under certain transformations.

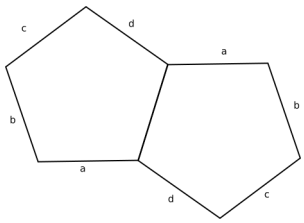

3 The Veech group

Definition 45. An *affine automorphism* of a translation surface X is a homeomorphism $\phi : X \to X$ such that

(i) ϕ permutes the nontrivial cone points of X

(ii) Every ordinary point of X has a neighborhood in which ϕ is an affine map

The group of all affine automorphisms of a surface X is denoted by $\mathrm{Aff}(X)$. Of particular interest is the subgroup which preserves orientation, denoted by $\mathrm{Aff}^+(X)$.

Definition 46. The *Veech group* of a translation surface X, denoted by $\Gamma(X)$, consists of derivatives of affine automorphisms of the surface.

The Veech groups $\Gamma(X_8)$ and $\Gamma(X_5)$ were identified by Veech in his original paper. They are the subgroups of $SL(2,\mathbb{R})$ generated by the matrices

$$R_n = \begin{pmatrix} \cos(2\pi/n) & -\sin(2\pi/n) \\ \sin(2\pi/n) & \cos(2\pi/n) \end{pmatrix}$$

and

$$T_n = \begin{pmatrix} 1 & \lambda_n \\ 0 & 1 \end{pmatrix}$$

where $\lambda_n = 2\cot(\pi/n)$, and $n = 8$ or 5.

The transformation represented by R_n is a counter-clockwise rotation by angle $2\pi/n$, while T_n corresponds to a horizontal shear, in this context often referred to as a *Dehn twist*. On a regular n-gon translation surface where n is even, the rotation is applied in the obvious way to the polygon in the gluing construction. On a double n-gon surface, such as X_5, the rotation is applied to each n-gon individually.

The affine automorphism A_T with derivative T_n is a less obvious transformation of the surface. On the polygon, T_n fixes a set of parallel lines joining its vertices. These lines partition the surface into cylinders, i.e. rectangles whose 2 horizontal boundary components are distinct but whose vertical boundary components are identified. Such a partition of a translation surface is known as a cylinder decomposition.

To illustrate, take X_8 and consider the cylinder decomposition indicated in the figure. Let P be the polygon from which X_8 is constructed, and let $\frac{1}{c}$ be the distance from the center of P one of its vertices. Let h_i and w_i denote the height and width, respectively, of cylinder I. Then some simple trigonometry gives us

$$h_1 = c \cdot (1 - \frac{\sqrt{2}}{2})$$

$$h_2 = c \cdot (\frac{\sqrt{2}}{2})$$

$$w_1 = c \cdot (\sqrt{2})$$

$$w_2 = c \cdot (2 + \sqrt{2})$$

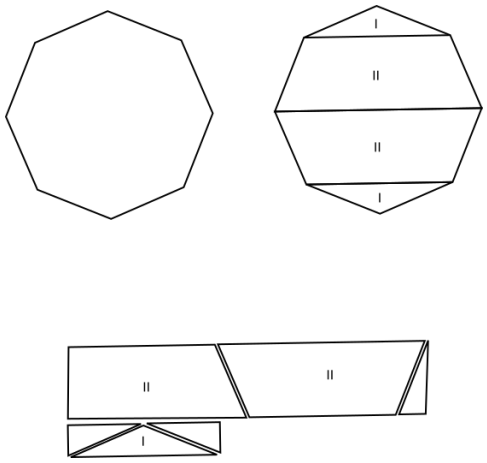

Figure 1: cylinder decomposition of the regular octagon

This lets us compute the *modulus* of each cylinder, which is the ratio of a cylinder's height to its width, or equivalently, the *inverse modulus*:

$$\frac{w_1}{h_1} = \frac{w_2}{h_2} = 2 + 2\sqrt{2} = 2\cot\frac{\pi}{8}$$

For a surface to have a cylinder decomposition such that each cylinder has the same modulus is quite rare, but every regular n-gon translation surface has such a decomposition.[2]

The transformation A_T maps the cylinder I to $\mathbb{R}^2$ so that its vertices map to vectors

$$\begin{pmatrix} 0 \\ 0 \end{pmatrix}, \begin{pmatrix} w_1 \\ 0 \end{pmatrix}, \begin{pmatrix} 0 \\ h_1 \end{pmatrix}, \begin{pmatrix} w_1 \\ h_1 \end{pmatrix}$$

The linear part of A_T, represented by the matrix T_8, acts on the cylinder as indicated in the figure. Since the shear preserves area, the image of cylinder I can be cut, reglued, then mapped back to the surface.

The transformation acts similarly on cylinder II, twisting vertical segments within the cylinder once around horizontally.

4 $SL(2,\mathbb{R})$-orbits

This secion assumes familiarity with some fundamental results in algebraic topology. The relevant definitions and theorems are included in the appendix.

The group $SL(2,\mathbb{R})$ acts on the space of translation surfaces in the following way. Let (X,ω) be a translation surface, and let $A \in SL(2,\mathbb{R})$. Let $A\cdot\omega$ denote

[2]For a nice trigonometric proof of this, see [4]

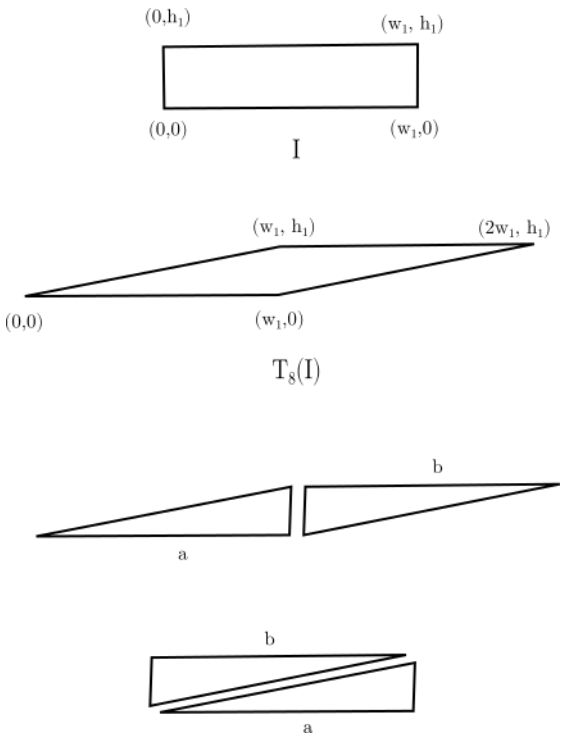

Figure 2: the twist applied to cylinder I

the atlas obtained by mapping each chart (U_ϕ, ϕ) to the chart $(U_{A\circ\phi}, A \circ \phi)$. This defines a group action of $SL(2,\mathbb{R})$ on the set of translation surfaces.

For a regular n-gon translation surface X_n, it can be shown that the stabilizer of X_n is precisely the Veech group $\Gamma(X_n)$.[3] This allows us to compute the orbits $SL(2,\mathbb{R})/\Gamma(X_n)$ explicitly.

4.1 The orbits of degree 2 covers of X_8

Let Y_1 and Y_2 be degree 2 coverings of X_8 with covering maps p_1 and p_2, and let $f \in \Gamma(X_8)$. It can be shown that $f \circ p$ lifts to an affine automorphism of Y_1 with Y_2 if and only if $f_*(p_{1*}(\pi_1(Y_1))) = (p_{2*}(\pi_1(Y)))$. This means that two coverings Y_1 and Y_2 are equivalent if and only if the images of their fundamental groups lie in the same orbit under the induced group homomorphisms g_*, where $g \in \Gamma(X_8)$.

For degree 2 coverings, the images of fundamental groups are kernels of homomorphisms from $\pi_1(X_8)$ onto $\mathbb{Z}/(2)$. Since these homomorphisms factor through the fundamental group's abelianization $H_1(X_8)$, we can determine these orbits by examining the induced action of $\Gamma(X_8)$ on the first cohomology $H^1(X_8, \mathbb{Z}/(2)) = \mathrm{Hom}(H_1(X_8), \mathbb{Z}/(2))$.

The explicit correspondence is this: let Y_1 and Y_2 be degree 2 coverings of X_8, let $K_i = p_{i*}(\pi_1(Y_i))$, such that K_i is the kernel of a group homomorphism $\phi_i : H_1(X_8) \to \mathbb{Z}/(2)$. Then there is some $f \in \Gamma(X_8)$ so that $f^*(\phi_1) = \phi_2$.

Since $H_1(X_8)$ is isomorphic to $\mathbb{Z}^4$, we will compute the orbits of $\phi \in H^1(X_8, \mathbb{Z}/(2))$ by representing the generators R_8 and T_8 of $\Gamma(X_8)$ as integer matrices R^* and T^*, then applying these to each nonzero element $v \in \mathbb{Z}^4$. [4] The resulting triples $(v, R^*(v), T^*(v))$ can then be used to construct a graph whose connected components will correspond to the orbits.

4.2 The matrices R^* and T^*

To construct R^* and T^*, we let $x \in X_8$ be the sole cone point, and choose as a basis of $H_1(X_8, x)$ the images of 4 loops corresponding to 4 adjacent directed edges of the octagon v_1, v_2, v_3, v_4 so that the head of v_i is the tail of v_{i+1}. The remaining edges then correspond to the inverses $-v_1, -v_2, -v_3, -v_4$.

The rotation maps v_i to v_{i+1} for $i = 1, 2, 3$, and v_4 is mapped to $-v_1$. If we represent $v_1, ..., v_4$ as the standard basis vectors in $\mathbb{Z}^4$, then R is given by the matrix

[3] See [3]

[4] These are actually elements of the module dual to $H^1(X_8, \mathbb{Z}/(2))$, but computing these orbits will still give us the equivalence classes we want.

$$R^* = \begin{pmatrix} 0 & 0 & 0 & 1 \\ 1 & 0 & 0 & 0 \\ 0 & 1 & 0 & 0 \\ 0 & 0 & 1 & 0 \end{pmatrix}$$

The matrix T^* is somewhat more difficult to construct. Using the indicated cylinder decomposition, v_2 and v_3 are contained in cylinder I, while v_1 and v_4 are contained in cylinder II.

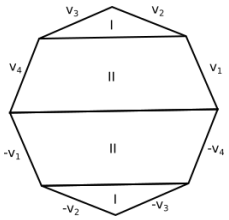

The tail of the vector $-v_3$ is fixed by the twist, and its head travels once around the cylinder. In terms of our basis, the image of $-v_3$ is $-v_3 - v_2 - v_3 = -v_2$, so that $v_3 \mapsto v_2$. The images of the remaining vectors are found analogously, resulting in the matrix

$$T^* = \begin{pmatrix} 0 & 0 & 0 & 1 \\ 0 & 0 & 1 & 0 \\ 0 & 1 & 0 & 0 \\ 1 & 0 & 0 & 0 \end{pmatrix}$$

By applying these two matrices to the fifteen nonzero elements of $\mathbb{Z}/(2)^4$, we construct a graph with 15 vertices. The vertices are labelled $1, ..., 15$, each representing an element of $\mathbb{Z}/(2)^4$ interpreted as a 4-digit binary number.

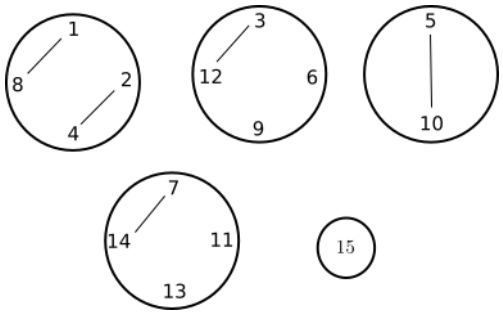

The vertices contained within a circle here correspond to orbits under the action of the rotation. Traveling clockwise around the circle corresponds to an application of R^*. A line segment joining two vertices corresponds to applying T^*. Isolated vertices within a circle correspond to vectors stabilized by the twist, i.e. eigenvectors of T^* with eigenvalue 1.

This graph gives us the 5 equivalence classes of degree 2 covers of X_8. In particular, there is a single degree 2 cover whose orbit contains no other cover. Since the Veech group of this cover Y is the stabilizer subgroup of of $\Gamma(X_8)$, we have that $\Gamma(Y) = \Gamma(X_8)$. This agrees with a theorem of Hubert and Schmidt [5] which says that every regular $2n$-gon X_{2n} has a degree 2 cover $X_{2n,2}$ which is a double $2n$-gon whose Veech group is the same as that of X_{2n}.

4.3 Orbits of degree 2 covers of X_5

Applying the same method to the double pentagon surface, we can construct matrices R^* and T^* to obtain another graph with 15 vertices whose connected components correspond to affine equivalence classes of degree 2 covers of X_5.

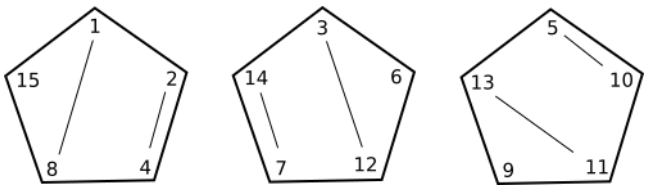

Each of the pentagons here corresponds to an orbit of the rotation, and again, traveling clockwise around the pentagon corresponds to applying the rotation. A line segment joining two vertices within a pentagon corresponds to applying the twist.

That there are 3 orbits here agrees with the results of Finster [3], who has computed the orbits of degree d covers of X_5 for $d = 2, ..., 5$. But this and other properties of this group action are actually easy to infer without constructing the graph. Instead, we examine the rotation matrix:

$$R^* = \begin{pmatrix} 0 & 0 & 0 & 1 \\ 1 & 0 & 0 & 1 \\ 0 & 1 & 0 & 1 \\ 0 & 0 & 1 & 1 \end{pmatrix}$$

It is clear that the orbit of the first standard basis vector under this matrix will consist of the ramaining standard basis vectors and the vector $(1, 1, 1, 1)$. This implies that the vectors $(1, 1, 0, 0)$ and $(1, 0, 1, 0)$ will also have orbits of order 5, and that these will be distinct.

5 Other double-n-gon translation surfaces

We conclude with a conjecture which generalizes the discussion of the previous section. Using the same method, we construct the matrices R^* and T^* for the double-n-gon translation surfaces where $n = 7$ and $n = 9$. In each case, the matrices are of the following form:

$$R^* = \begin{pmatrix} 0 & \dots & \dots & 0 & 1 \\ 1 & 0 & \dots & 0 & 1 \\ 0 & \ddots & 0 & 0 & 1 \\ 0 & \dots & 0 & 1 & 1 \end{pmatrix}$$

$$T^* = \begin{pmatrix} 0 & \dots & 0 & 1 \\ \vdots & & \iddots & 0 \\ 0 & \iddots & & \vdots \\ 1 & 0 & \dots & 0 \end{pmatrix}$$

Conjecture 20. *Let X_n be a double-n-gon translation surface, n odd. Let Y be a degree 2 cover of X_n. Then $\Gamma(X_n) \neq \Gamma(Y)$.*[5]

6 Appendix

6.1 Algebraic topology

All definitions here can be found in [2]

Definition 47. Let X be a topological space with $x \in X$. The fundamental group $\pi_1(X, x)$ is defined to be the set of homotopic loops in X with basepoint x, with the following multiplication: for two equivalence classes $[f], [g]$, define $[f] \cdot [g]$ by $[f \cdot g]$, where f and g are representatives of $[f]$ and $[g]$, and $f \cdot g$ is given by

$$f \cdot g(t) = g(2t), \text{ for } t \in [0, 1/2]$$

and

$$f \cdot g(t) = f(2t), \text{ for } t \in [1/2, 1]$$

Definition 48. Let X, Y be topological spaces and let $f : Y \to X$ be a continuous surjective map. An open set $U \subset X$ is *evenly covered* by f if $f^{-1}(U)$ consists of a countable union of disjoint open sets V_α such that $f(V_\alpha)$ is a homeomorphism of V_α onto U.

Definition 49. A *covering space* of a topological space X is a space Y together with a continuous map $p : Y \to X$ such that every point $x_0 \in X$ has a neightborhood which is evenly covered by p.

Definition 50. Let X, Y be topological spaces and let Y be path-connected and locally path-connected. Let C be a covering space with covering map $p : C \to X$. Let $f : Y \to X$ be a continuous map. A *lift* of f is a continuous map $f' : Y \to C$ such that $p \circ f' = f$.

[5] This may be known already, but I couldn't find it in the literature.

Theorem 21. *Let X, Y be topological spaces and let Y be path-connected and locally path-connected. Let C be a covering space with covering map $p : C \to X$. Let $f : Y \to X$ be a continuous map, and let $f(y_0) = p(c_0) = x_0$ for $y_0 \in Y, c_0 \in C, x_0 \in X$. Then there exists a unique lift $f' : X \to C$ such that $f'(y_0) = c_0$ if and only if*

$$f_*(\pi_1(Y, y_0)) \subset p_*(\pi_1(C, c_0))$$

Theorem 22. *Let $p : E \to B$ be a covering map; let E be path connected; let $p(e_0) = b_0$. Then*

- *(a) $p_* : \pi_1(E, e_0) \to \pi_1(B, b_0)$ is injective.*
- *(b) There is a bijection*

$$\phi : \pi_1(B, b_0)/H \to p^{-1}(b_0),$$

where $H = p_*(\pi(E, e_0))$ and $\pi(B - b_0)/H$ is the collection of right cosets of H in $\pi_1(B, b_0)$.

Corollary 23. *Let $f : X \to X$ be an automorphism of a path-connected and locally path-connected space X, and let Y be a covering space of X. Then f lifts to an automorphism of Y if and only if $f_*(p_*(\pi_1(Y, y_0))) \subset p_*(\pi_1(Y, y_0))$.*

This implies that an element $f \in \Gamma(X)$ lifts to an element of $\Gamma(Y)$ if and only if $f_* \in \mathrm{Stab}(p_*(\pi_1(Y, y_0)))$.

Theorem 24. *The fundamental group of a compact orientable surface of genus 2 is isomorphic to the group*

$$< a, b, c, d \mid abcda^{-1}b^{-1}c^{-1}d^{-1} = 1 >$$

Theorem 25. *A compact, orientable surface of genus 2 has exactly 15 degree 2 covers.*

Proof. (Sketch). Let $G = \pi_1(X, x_0)$ be the fundamental group of a genus 2 surface, and let g_1, g_2, g_3, g_4 be generators of G. Define a map $\phi : G \to \mathbb{Z}/(2)$ by setting $\phi(g_i) = 0$ or $\phi(g_i) = 1$ for $i = 1, 2, 3, 4$. Then ϕ can be extended to a group homomorphism in the obvious way. To verify that ϕ is a homomorphism, we need only check that the relator

$$g_1 g_2 g_3 g_4 g_1^{-1} g_2^{-1} g_3^{-1} g_4^{-1}$$

is mapped to the identity:

$$\begin{aligned} &\phi(g_1 g_2 g_3 g_4 g_1^{-1} g_2^{-1} g_3 - 1 g_4^{-1}) \\ &= \phi(g_1)\phi(g_2)\phi(g_3)\phi(g_4)\phi(g_1)^{-1}\phi(g_2)^{-1}\phi(g_3)^{-1}\phi(g_4)^{-1} \\ &= \phi(g_1)\phi(g_1)^{-1}\phi(g_2)\phi(g_2)^{-1}\phi(g_3)\phi(g_3)^{-1}\phi(g_4)\phi(g_4)^{-1} = 0 \end{aligned}$$

All but one of these 16 maps is surjective, so the kernels are exactly the 15 index 2 subgroups of G. □

6.2 Miscellanious Proofs

Theorem 26. *If n is odd then the regular $2n$-gon translation surface has 2 cone points.*

Proof. Recall that this surface is constructed by identifying parallel edges. If we cyclically order the $2n$ vertices $v_1, ..., v_{2n}$, then such an identification maps the edge $v_{i-1}v_i$ to $v_{k-1}v_k$, where $k = i + n \mod 2n$. Note that the vertex with index i is mapped to that of index $i+n-1 \mod 2n$. This means we can find all vertices identified with v_i by finding the orbit of an arbitrary element $i \in \mathbb{Z}/(2n)$ under repeated addition by $n-1$. But since n is not divisible by 2, $n(n-1)$ is divisible by both 2 and n, hence it is congruent to 0 mod $2n$. Since the order of i under this action must divide $2n$ and since the order is not 2, the order is exactly n, so there are n elements in the orbit of i. This means that there are 2 sets of vertices of the $2n$-gon corresponding to 2 distinct points in the surface obtained. □

References

[1] Richard Schwarz, *Mostly Surfaces*, American Mathematical Society, Rhode Island, 2011.

[2] James Munkres, *Topology: A First Course*, Prentice-Hall, New Jersey, 1975.

[3] Myriam Finster, *Veech Groups and Translation Coverings*, KIT Scientific Publishing, Karlsruhe, 2014.

[4] Myriam Finster, *A series of coverings of the regular n-gon*, ArXiv e-prints, 2010

[5] P. Hubert and T.A. Schmidt, *Invariants of translation surfaces*, Anales de l'institut Fourier 51 (2001) no. 2, 461-495.